Review | Open Access

Microstructures

Zhu et al. Microstructures 2026, 6, 2026076 DOI:10.20517/microstructures.2025.168

Flexible thermoelectric generators for wearable energy harvesting and applications

Jiaqi Zhu[1,#], Jiahao Zhou[2,#], Haitong Yang[1], Haihang Feng[1], Meiping Xu[1], Jinye Chen[1], Peidi Zhou[3], Chan Zheng[1], Minghua You[1], Mingcen Weng[1,4,5], Hanxiao Shao[6], Huamin Chen[6]

Keywords:
Thermoelectric materials, flexible thermoelectric generators, energy harvesting, nanostructured materials, wearable electronics

Citation: Zhu, J.; Zhou, J.; Yang, H.; Feng, H.; Xu, M.; Chen, J.; Zhou, P.; Zheng, C.; You, M.; Weng, M.; Shao, H.; Chen, H. Flexible thermoelectric generators for wearable energy harvesting and applications. *Microstructures* **2026**, *6*, 2026076. https://dx.doi.org/10.20517/microstructures.2025.168

Received: 17 Dec 2025
First Decision: 3 Feb 2026
Revised: 13 Feb 2026
Accepted: 20 Mar 2026
Published: 2 Jun 2026

Academic Editor:
Zhi-Gang Chen
Copy Editor:
Ping Zhang
Production Editor:
Ping Zhang

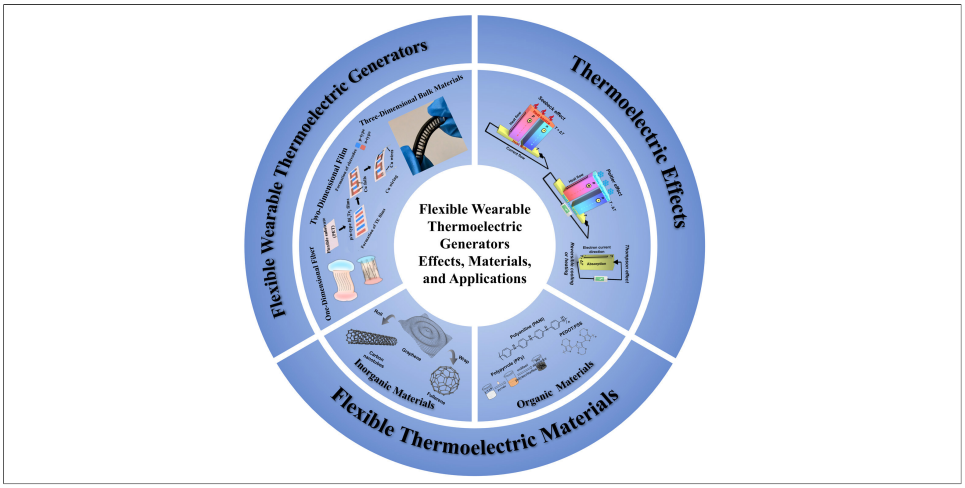

Abstract

Thermoelectric materials are critical for high-efficiency energy utilization and carbon neutrality. With the booming development of wearable electronics, flexible sensor networks and smart textiles, flexible thermoelectric generators (f-TEGs) have garnered immense interest for self-powered health monitoring and personalized thermal management. Focusing on wearable feasibility, this review summarizes the fundamental thermoelectric physics and performance metrics. It also highlights recent advances in flexible materials - including inorganic (carbon nanomaterials, chalcogenides), organic [polyaniline, polypyrrole, poly(3,4-ethylenedioxythiophene) (PEDOT), and composites], and inorganic-organic hybrid systems - with an emphasis on structure-property relationships and wearable-adapted processing. At the device level, the review compares fiber/yarn, film/ribbon, and porous/textile-like architectures. It focuses on heat transfer,

[1]Institute of Biology and Chemistry, Fujian University of Technology, Fuzhou 350118, Fujian, China.
[2]Key Laboratory of Molecule Synthesis and Function Discovery (Fujian Province University), College of Chemistry, Fuzhou University, Fuzhou 350108, Fujian, China.
[3]Key Laboratory of Marine Smart Equipment (Fujian University of Technology), School of Smart Marine Science and Technology, Fujian University of Technology, Fuzhou 350118, Fujian, China.
[4]Department of Physics, Tianjin University, Tianjin 300350, China.
[5]Sanxiang Advanced Materials Co., Ltd., Ningde 355500, Fujian, China.
[6]Institute of Semiconductors, Chinese Academy of Sciences, Beijing 100083, China.
[#]These authors are contributed equally to this work.

Correspondence to: Prof. Chan Zheng, Dr. Minghua You, Prof. Mingcen Weng, Institute of Biology and Chemistry, Fujian University of Technology, Fuzhou 350118, Fujian, China. E-mail: czheng@fjut.edu.cn; yyomh@fjut.edu.cn; wengmc@fjut.edu.cn; Prof. Huamin Chen, Institute of Semiconductors, Chinese Academy of Sciences, Beijing 100083, China. E-mail: chenhuamin@semi.ac.cn

mechanical durability, and skin comfort, which are critical for on-skin applications. Key wearable-specific bottlenecks are outlined, such as stable n-type materials, scalable fabrication, and environmental/biological durability. Finally, it proposes opportunities for application-oriented f-TEG platforms, facilitating the development of next-generation wearable energy-harvesting systems through interdisciplinary collaboration.

INTRODUCTION

Thermoelectric materials can directly and reversibly convert heat into electricity across a temperature gradient and have emerged as a key class of functional materials for high-efficiency energy utilization and carbon neutrality[1,2]. Compared with conventional electromechanical power generation or refrigeration technologies, thermoelectric conversion does not require mechanical moving parts and offers clear advantages such as compact structure, rapid response, low noise, high reliability and easy miniaturization and integration. These merits have sparked broad interest in thermoelectric materials for sustainable energy harvesting and solid-state cooling, and have increasingly aligned the field with the development of flexible and wearable technologies including self-powered sensing, smart textiles, and human-centric thermal management[3-5]. Benefiting from continuous progress in materials design and nanoscale structural engineering, the dimensionless figure of merit thermoelectric figure of merit (ZT) of classical bulk inorganic thermoelectric materials such as Bi_2Te_3, PbTe and SnSe has been significantly improved in both room-temperature and mid-temperature ranges, providing a solid foundation for high-efficiency thermoelectric energy conversion[3,6,7]. However, these traditional bulk inorganic materials are generally characterized by high modulus, pronounced brittleness and relatively large density, making them difficult to withstand routine bending, twisting or tensile deformation[8,9]. As a result, they exhibit clear limitations in structural adaptability and service compatibility for flexible electronics and wearable applications.

In parallel, the rapid development of wearable electronics, flexible sensing networks, smart textiles and continuous health-monitoring systems has imposed more stringent requirements on safe, stable, and sustainable microscale power sources[10,11]. Low-grade heat flows on human skin, in ambient air streams, and around operating electronic devices are typically broad in spatial distribution and long in time scale, and modest in energy density. Conventional battery-powered supplies not only raise maintenance costs and environmental burden, but also limit truly unobtrusive wear and long-term autonomous operation of devices. Against this backdrop, flexible thermoelectric generators (f-TEGs) harvest low-grade heat and convert it into electricity by establishing a temperature difference between the human body, environment, and the device. These devices offer a promising self-powered solution for wearable systems, eliminating the need for frequent battery replacement, and serve as a key energy interface between human thermal resources and the flexible electronics ecosystem[12,13]. Compared with photovoltaics[14,15], piezoelectrics[16,17], triboelectrics[18,19], and other energy-harvesting approaches, flexible thermoelectric technologies do not depend on light or vigorous motion. They can operate stably around the clock - both indoors and outdoors - and under static or mildly dynamic conditions.

Numerous of reviews on thermoelectric materials and f-TEGs have been published, but most focus on either material-level fundamental properties (e.g., ZT optimization) or general device design, with little attention to wearable-specific demands and practical applicability. Existing reviews typically classify systems by material type (inorganic/organic/composite) or device dimensionality [one-dimensional (1D)/two-dimensional (2D)/three-dimensional (3D)]. This classification separates components from application scenarios and fails to meet the core needs of wearable electronics. In contrast, this review distinguishes itself by centering on "wearable feasibility" as its core logic, and constructs a human-centric framework that links material design, device architecture, and application around wearable-specific challenges. Against this backdrop, a systematic overview of flexible thermoelectric materials and flexible wearable thermoelectric generators is crucial for

Table 1. Key thermoelectric properties of different flexible thermoelectric material systems

Materials	Material classification	n/p type	*ZT*	S (μV K^{-1})	σ (S cm^{-1})	κ (W m^{-1} K^{-1})	Ref.
PEDOT:PSS films	Organic	p	0.3	21.9	2,980	0.22	[20]
PEDOT:PSS ink	Organic	p	-	16-17	5.847	-	[21]
PEDOT:PSS-rGO	Organic	p	-	60	-	-	[22]
CNT/P3HT	Organic	p	-	41.8	1,170	-	[23]
$Bi_{0.4}Sb_{1.6}Te_3$	Inorganic	p	0.04	150	-	1.1	[24]
Bi_2Te_3 film	Inorganic	n	-	-37	-	-	[25]
Na-doped PbTe	Inorganic	p	1.4	295.3	10^2-10^3	0.8	[26]
Sb-doped PbTe	Inorganic	n	1.2	-227.6	10^2-10^3	0.65	[26]
Te/PEDOT film	Organic- inorganic	P	-	42	-	-	[27]
Cu_2S/PEDOT:PSS	Organic- inorganic	P	-	33	192.17	-	[28]
PVP/Ag_2Se	Organic- inorganic	n	1.1	-143	929	0.508	[29]
CNT yarn + PEI	Organic- inorganic	n	-	-68.7	1,408.3	35	[30]

PEDOT: poly(3,4-ethylenedioxythiophene); PSS: polystyrene sulfonate; CNT: carbon nanotube; P3HT: poly(3-hexylthiophene); *ZT*: thermoelectric figure of merit; PEI: polyethyleneimine.

clarifying the intrinsic correlations among structure, performance and application, identifying key bottlenecks and guiding future research directions. In this review, we first provide a brief recap of the physical mechanisms of the thermoelectric effect and the core performance metrics, thereby laying the theoretical basis for the design of flexible thermoelectric materials and devices. We then focus on three aspects: (i) materials-design strategies and performance-modulation rules for inorganic flexible thermoelectric systems, conducting polymers and their composites; (ii) structural characteristics, fabrication techniques, and representative application scenarios of different flexible device architectures - including 1D fibers and yarns, 2D films and ribbons, and 3D microstructured devices; (iii) the latest advances and trends of flexible wearable thermoelectric systems in human-body heat harvesting, self-powered health monitoring and multifunctional, multi-field-coupled applications. Finally, we discuss the remaining challenges associated with large-area manufacturing, long-term stability, biocompatibility and system integration. We also offer an outlook on future research priorities and application prospects of flexible thermoelectric materials and wearable thermoelectric generators, aiming to provide guidance for the development of next-generation high-performance, engineering-ready flexible thermoelectric energy solutions.

FLEXIBLE THERMOELECTRIC MATERIALS

Flexible thermoelectric materials are the material core of f-TEGs for wearable energy harvesting, whose thermoelectric performance directly determines the energy conversion efficiency of devices, and whose mechanical properties affect their wearable adaptability. Table 1 summarizes the key thermoelectric properties [e.g., *ZT*, the Seebeck coefficient (S), electrical conductivity (σ), and total thermal conductivity (κ)] of mainstream organic, inorganic, and organic-inorganic composite flexible thermoelectric materials. It intuitively reflects their performance differences and providing a basis for the subsequent detailed analysis of each material system.

Inorganic thermoelectric materials

Owing to their excellent thermoelectric performance, inorganic thermoelectric materials have long held an important position in the field of efficient thermoelectric conversion. Especially in flexible thermoelectric device applications, inorganic materials, inorganic materials exhibit stronger competitiveness than organic materials due to their outstanding Seebeck coefficients and electrical conductivities[13,31,32]. However, traditional inorganic materials are often highly rigid, limiting their application in wearable electronics and

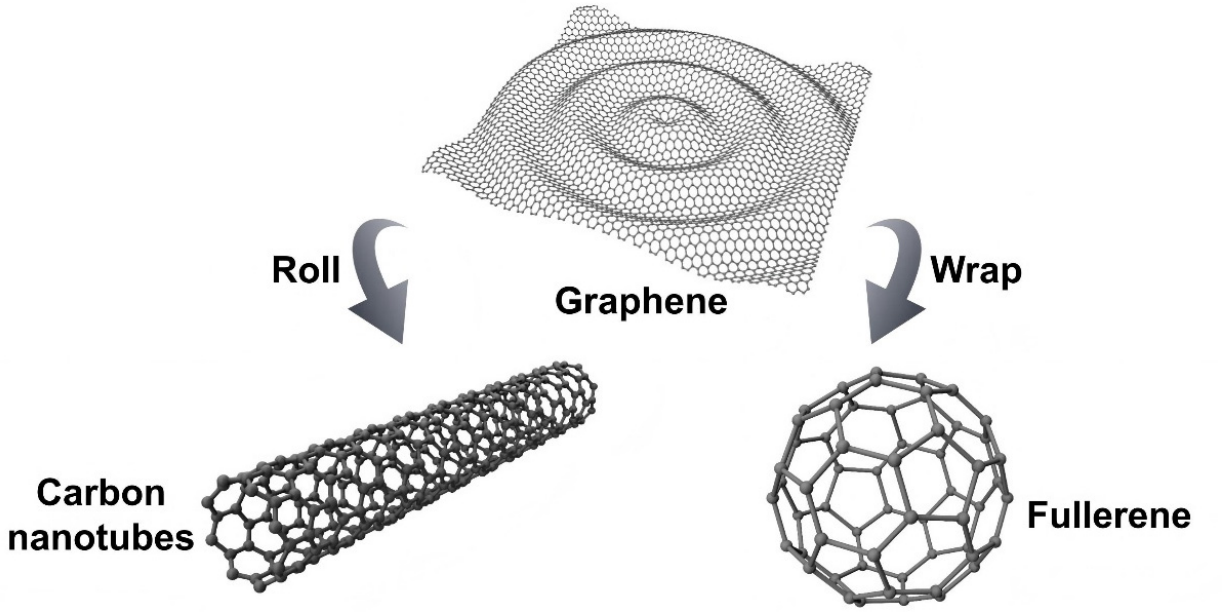

Figure 1. Schematic diagram of the structure of zero-, one-, two- and three-dimensional carbon nanomaterials.

flexible devices. Therefore, enabling inorganic materials to be flexible and bendable through structural optimization, nanostructuring, and interface engineering has become a research focus.

Current research on flexible inorganic thermoelectric materials mainly concentrates on two major systems: carbon nanomaterials and chalcogenides. These two material types have distinct advantages and challenges. Various innovative strategies have been adopted to optimize their thermoelectric performance and enhance their flexibility. The following section details the research progress of these two inorganic thermoelectric materials types and their application potential in flexible thermoelectric devices.

Carbon-nanomaterial thermoelectric

Carbon nanomaterials, including graphene, carbon nanotubes (CNTs) and fullerenes [Figure 1][33,34], have emerged as promising candidates for flexible thermoelectric materials due to their excellent electrical conductivity, mechanical properties, and thermal stability. In particular, graphene, as a two-dimensional material, has made remarkable progress in flexible thermoelectric device research in recent years due to its ultrahigh electrical conductivity and outstanding thermoelectric performance. CNTs, especially single-walled carbon nanotubes (SWCNTs) and multi-walled carbon nanotubes (MWCNTs), also play an important role in flexible thermoelectric material development due to their tunable conductivity and high flexibility. Fullerenes are carbon allotropes with cage-like structures. They are widely used in thermoelectric, electronics, and materials science for their unique properties.

Structural regulation strategies, such as doping, nanostructuring, and composite design, have significantly improved the thermoelectric performance of carbon nanomaterials. For example, graphene/CNT composites exhibit excellent power factors. These composites combine the high electrical conductivity of graphene with the excellent thermoelectric response of CNTs, fully leveraging the synergistic effect of the materials.

CNTs are tubular materials formed by carbon atoms linked via covalent bonds with sp^2 hybridization into hexagonal units. Carbon atoms form a conjugated electron cloud via a pair of unhybridized p electrons extending across the CNTs. Based on the number of layers in their tubular structure, CNTs can be divided

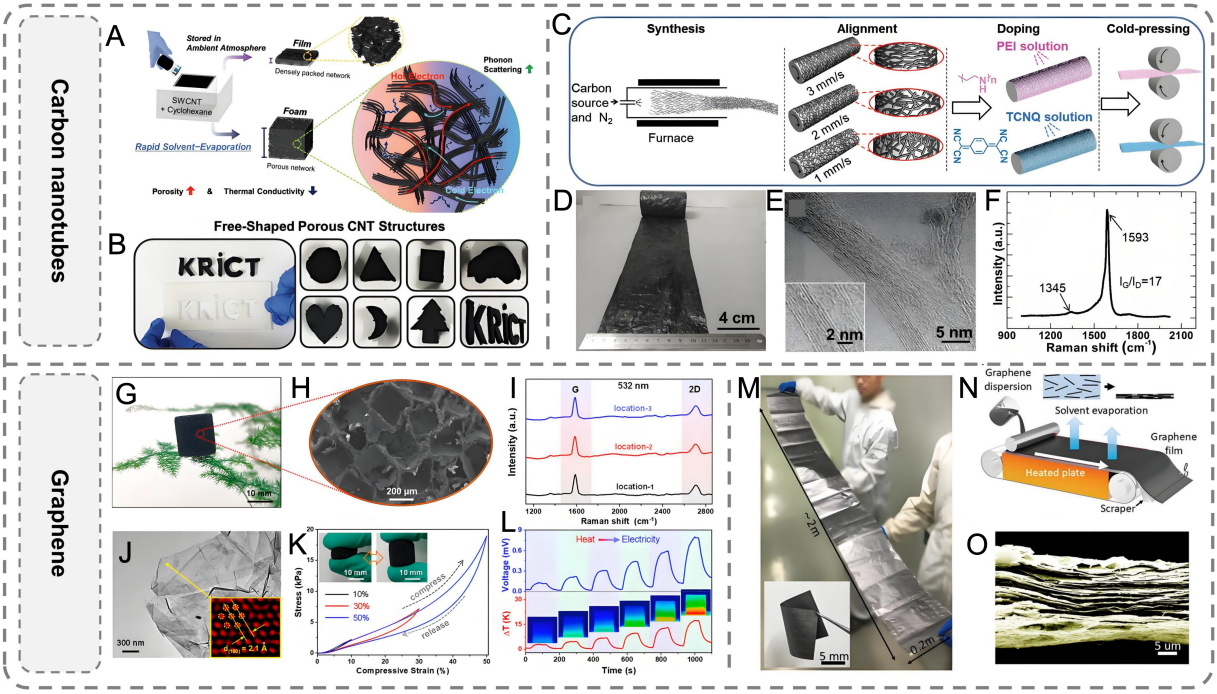

Figure 2. (A) Preparation process of the CNTs aerogel; (B) images of CNTs aerogel fabricated using template method. (A and B) Reproduced with permission[37]. Copyright 2019, WILEY-VCH; (C) Synthesis and modification of MWCNTs by CVD, (D) photographs of large-size MWCNTs film, (E) TEM image of MWCNTs, (F) Raman spectroscopy of MWCNTs. (C-F) Reproduced with permission[39]. Copyright 2022, WILEY-VCH; (G and H) Morphology, (I) Raman spectra and (J) TEM image of graphene-based aerogels, (K) stress-stain curve and (L) TE responses of graphene aerogel. (G-L) Reproduced with permission[47]. Copyright 2022, American Chemical Society; (M) Optical photographs, (N) preparation process and (O) Raman spectra film. (M-O) Reproduced with permission[48]. Copyright 2019, Elsevier Ltd. CNTs: Carbon nanotubes; MWCNTs: multi-walled carbon nanotubes; CVD: chemical vapor deposition; TEM: transmission electron microscope; TE: thermoelectric; SWCNT: single-walled carbon nanotube; TCNQ: tetracyanoquinodimethane; PEI: polyethyleneimine.

into SWCNTs and MWCNTs[35,36]. The application of CNTs in flexible thermoelectric devices has been extensively studied. In particular, for preparing thermoelectric aerogels, their excellent electrical conductivity and tunability make them ideal candidates.

Thermoelectric aerogels constructed from CNTs exhibit high conductivity and, owing to their thickness advantage, can directly capture heat energy along the temperature-gradient direction, making them ideal flexible thermoelectric materials. CNT aerogels can be constructed via a simple, rapid-evaporation process. For example, Lee *et al.* constructed three-dimensional MWCNT aerogels using a rapid solvent-evaporation method. The fabrication flowchart and various aerogel morphologies are shown in Figure 2A and B[37]. Controlling the concentration of MWCNTs in the slurry enables the preparation of aerogels with different densities and pore diameters.

Although the porous structure of aerogels can effectively reduce thermal conductivity, it also results in relatively low electrical conductivity. In contrast, CNT films exhibit significantly higher electrical conductivity. In addition to high electrical conductivity, CNT films have a key advantage - large-scale production can be achieved via chemical vapor deposition (CVD), which lays an important foundation for the commercial application of thermoelectric materials. For example, Shi *et al.* fabricated Ag_2Se/MWCNTs composite films via screen printing. In these films, Ag_2Se nanoparticles bridge MWCNT networks, achieving a room-temperature power factor of 168 μW m^{-1} K^{-2} and a thermal conductivity of 0.28 W m^{-1} K^{-1}. The composite retains 88% of its initial conductivity after 800 bending cycles (R = 5 mm), making it suitable for

photothermoelectric integration in wearable devices[38]. Sun *et al.* used thiophene as the carbon source, ferrocene as the catalyst, and nitrogen gas as the protective atmosphere, respectively, and synthesized MWCNTs in batches via a high-temperature floating CVD method [Figure 2C]. Large-area oriented CNT films were collected using a rotating roller [Figure 2D]. In Figure 2E, the average inner diameter of the MWCNTs is approximately 2 nm, and the outer diameter is approximately 5 nm. Raman spectroscopy confirms the structural characteristics of MWCNTs, and a low I_G/I_D ratio verifies their low carbon defect advantage [Figure 2F][39].

In 2004, physicists Geim and Novoselov from the University of Manchester, UK obtained single-layer graphene from graphite via mechanical exfoliation[40,41], marking the birth of the first two-dimensional material and igniting a global research boom on two-dimensional materials. Graphene is a two-dimensional nanosheet formed by carbon atoms arranged in a hexagonal honeycomb structure via sp^2-hybridized orbitals. The thickness of single-layer graphene is approximately 0.335 nm, approaching the thickness of a single carbon atom[42,43]. In the six-membered carbon ring of graphene, each carbon atom is bonded to three neighboring carbon atoms via σ bonds. The π electrons not participating in σ bonding interact with those of other carbon atoms to form a large delocalized π bond, endowing graphene with excellent electrical properties by enabling electrons to move freely within its crystal structure. Owing to its long-range π-π conjugated structure, graphene exhibits numerous outstanding properties, including high chemical stability, high mechanical performance, and tunable thermal conductivity[44,45]. Building on improved graphene preparation, tailoring, and modification methods, large-area, high-quality graphene with precisely controlled patterns and specific functional groups can be used to fabricate devices. These advances will promote in-depth research on graphene's novel structures and electronic devices - such as magic-angle graphene and graphene-based single-molecule junctions - to facilitate the exploration of graphene's novel properties and applications[46].

Current forming processes can be used to prepare graphene into a series of macroscopic bulk materials. Based on structural and morphological differences, these macroscopic materials are mainly divided into three categories: 3D aerogels, 2D films, and 1D fibers. Graphene aerogels used in the thermoelectric field are mainly constructed via template methods, including polymer-template and ice-template methods. For example, Zhang *et al.* used polydimethylsiloxane (PDMS) as the skeleton and mixed bulk NaCl into a graphene/PDMS mixed solution to serve as a template. The characterization and properties of the thermoelectric (TE) sponges are shown in Figure 2G-L[47]. Owing to the extremely high fracture strength of PDMS, the graphene-based aerogel was endowed with excellent mechanical properties. It could still effectively maintain good morphological integrity and resistance stability during repeated compression cycles.

Unlike the CVD method for preparing large-area CNT films, the mass preparation of graphene films mainly relies on slurry-forming methods. For example, Feng *et al.* used a graphene dispersion with a concentration of 25 mg mL^{-1} as the slurry, cast it on a conveyor belt moving at constant speed, controlled the thickness of the gel-state slurry with a roller, and obtained large-size layered graphene films after heating, drying, and peeling [Figure 2M-O][48]. Scanning electron microscopy (SEM), Raman spectroscopy, and X-ray diffraction (XRD) confirm that graphene films prepared via the doctor-blading process exhibit good uniformity. Based on graphene's conduction mechanism, the Wiedemann-Franz law, and Mott's law, further optimization of carrier concentration can enable graphene's room-temperature power factor to exceed 200 μW cm^{-1} K^{-2}. To reduce thermal conductivity, Guo *et al.* prepared layered graphene oxide (GO) films with porous structures via the ice-template method and thermally reduced them in high-temperature N_2 and NH_3 atmospheres; N doping via NH_3 resulted in n-type conductive graphene materials. The continuous porous structure in graphene films can reduce the lattice thermal conductivity via phonon-scattering mechanisms[49]. In addition,

the porous structure increases the contact barrier between graphene nanosheets and enhances the energy-filtering effect, slightly increasing the Seebeck coefficient of graphene films. Furthermore, they assembled graphene films onto pre-stretched PDMS substrates. After release, graphene formed wrinkled structures on the PDMS film, thereby gaining stretchability. This pre-stretching process offers a new approach for the fabrication and structural design of flexible thermoelectric films.

Chalcogenide nano thermoelectric materials

Chalcogenide nanomaterials (e.g., Bi_2Te_3, PbTe) have long dominated the fields of thermoelectric power generation and refrigeration due to their excellent thermoelectric performance. In particular, Bi_2Te_3, as one of the most mature thermoelectric materials, exhibits optimal thermoelectric performance at room temperature and is widely used in thermoelectric power generation and refrigeration devices. However, traditional Bi_2Te_3 and other chalcogenide materials are limited for use in flexible and wearable thermoelectric devices due to their high rigidity and brittleness. Therefore, researchers have improved both the thermoelectric performance and flexibility of these chalcogenide materials via nanostructuring, alloying, doping, and interface engineering, making them more suitable for flexible thermoelectric devices[50].

VA_2-VIA_3 nanomaterials possess typical layered structures, with five atoms per layer arranged along the z-axis in the order VIA-VA-VIA-VA-VIA; adjacent layers are bonded via weak van der Waals forces[51-55]. The layered structure endows VA_2-VIA_3 materials with the ability to grow into atomic-layer-thick two-dimensional nanosheets, enabling directional regulation of their electrical, thermal, acoustic, and other physical and chemical properties. Current research on VA_2-VIA_3 thermoelectric materials mainly focuses on Bi_2Te_3, Sb_2Te_3, and Bi_2Te_3, as well as their modified derivatives; the room-temperature *ZT* values of bulk VA_2-VIA_3 materials have exceeded 1. Compared with bulk materials, nanostructured Bi_2Te_3, Sb_2Te_3, and Bi_2Te_3 can be assembled into flexible film materials via screen printing, inkjet printing, and slurry doctor-blading and other processes[51,52]. Thus, they are widely used in the flexible thermoelectric field.

As shown in Figure 3A, Shi *et al.* from the Changchun Institute of Applied Chemistry synthesized Sb_2Te_3 nanosheets with regular hexagonal structures via a solvothermal method; their edge length and thickness are approximately 800 and 78.5 nm, respectively. The schematic phase characterization of Sb_2Te_3 nanosheets is shown in Figure 3B-D[54]. Figure 3E-G show the temperature-dependent in-plane thermoelectric (TE) properties - including electrical conductivity, Seebeck coefficient, and power factor of flexible Sb_2Te_3 film printed on Kapton after sintering at 400 °C[52]. In the anisotropic layered structure of Sb_2Te_3, Sb and Te elements are arranged along the c-axis in the order -Te1-Sb-Te2-Sb-Te1-; van der Waals forces exist between adjacent Te1 layers, while covalent bonds connect Te and Sb atoms. Thus, Sb_2Te_3 nanosheets can be described as numerous crystalline planes extending vertically and connected by van der Waals bonds. From a thermodynamic perspective, the free energy required to break covalent bonds is higher than that required to break interlayer van der Waals forces. Thus, the growth rate of Sb_2Te_3 crystals along the upper and lower crystal planes is faster than that along the c-axis, ultimately forming a two-dimensional planar structure.

IB_2-VIA thermoelectric materials mainly include Ag_2Te, Cu_2Te, Ag_2Se, and Cu_2Se, as well as their modified derivatives; their main preparation methods are template methods and vacuum thermal evaporation[56-58]. IB_2-VIA thermoelectric materials can optimize their thermoelectric performance by controlling the Ag/Cu elements ratio to regulate carrier concentration; they can also achieve p-type and n-type conduction characteristics by changing the majority carrier type.

In the template method, nanowires or nanorods are first synthesized via a solvothermal process, followed by the growth of Ag and Cu metal elements within the nanowires. Thus, IB_2-VIA thermoelectric materials prepared via the template method generally exhibit one-dimensional wire-like morphologies. For example,

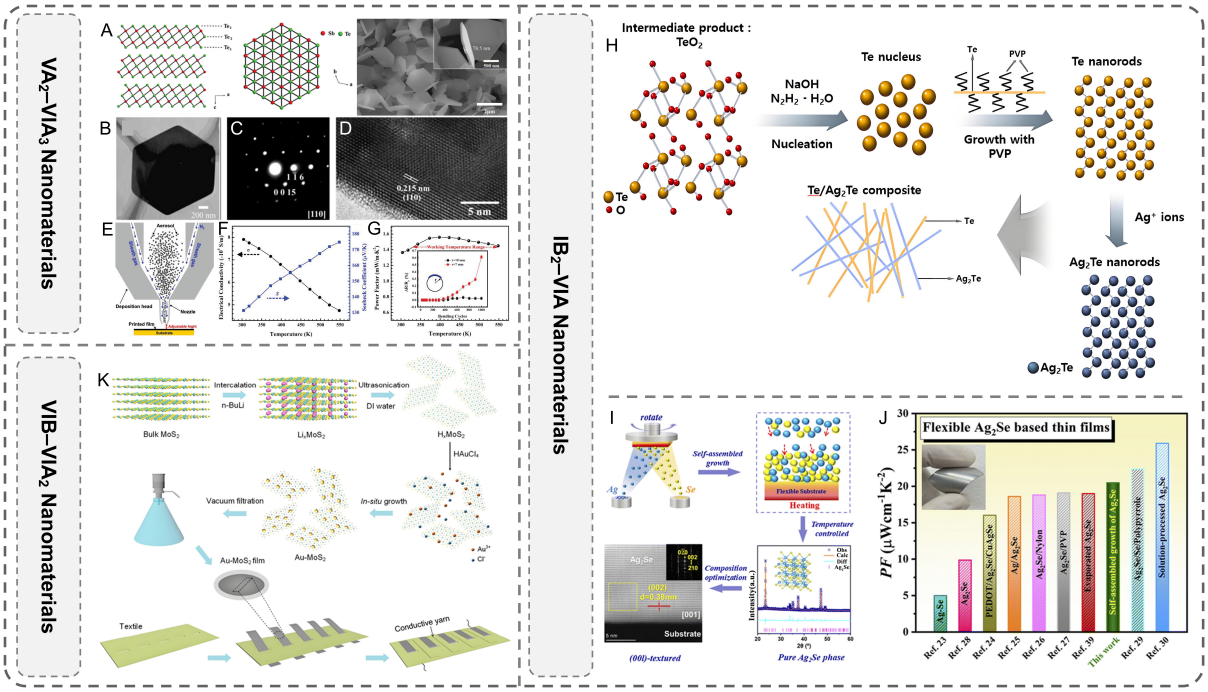

Figure 3. (A-D) Schematic structure and phase characterization of Sb_2Te_3 nanosheets. (A-D) Reproduced with permission[54]. Copyright 2008, WILEY-VCH; (E-G) 3D printing method to construct TE materials based on Sb_2Te_3 nanosheets and Temperature-dependent in-plane TE properties; (E-G) Reproduced with permission[52]. Copyright 2019, WILEY-VCH; (H) Growth mechanism of Te nanorods and Ag_2Te nanorods; (H) Reproduced with permission[58]. Copyright 2017, Elsevier Ltd and Techna Group S.r.l; (I) Schematic diagram of Ag_2Se thin film prepared by vacuum thermal evaporation method and (J) power factor comparison data; (I and J) Reproduced with permission[56]. Copyright 2022, Royal Society of Chemistry; (K) Fabrication of the flexible TE device. (K) Reproduced with permission[62]. Copyright 2018, American Chemical Society. TE: Thermoelectric.

Park *et al.* from Chung-Ang University, South Korea, synthesized Te nanorods via a solvothermal method and then modified them in an Ag precursor solution[58], preparing Ag_2Te nanomaterials with morphologies similar to those of the Te nanorods; the growth mechanisms of Te nanowires and Ag_2Te nanorods are shown in Figure 3H. Ag_2Te is an n-type narrow-band-gap semiconductor material with a room-temperature electrical conductivity of up to 200 S cm^{-1}. The wire-like structure not only optimizes thermoelectric performance but also lays a foundation for constructing flexible materials.

Unlike the template method, the vacuum thermal evaporation process can deposit bulk targets into nanomaterials and form various shapes via masks, making it suitable for application in the flexible thermoelectric field. As shown in Figure 3I and J, Zheng *et al.* used both Ag and Se ingots as targets; during vacuum thermal evaporation, excited Ag and Se atoms were deposited on a polyimide substrate and assembled into Ag_2Se films, respectively[56]. Adjusting the evaporation rates of Ag and Se atoms during vacuum evaporation enables the preparation of Ag_2Se materials with different atomic ratios. At 348 K, the optimized power factor can reach 19.6 μW cm^{-1} K^{-2}, which is close to the highest reported thermoelectric performance of Ag_2Se-based materials to date.

In addition to Ag- and Cu-based IB_2-VIA group compounds, p-type Mg_3Sb_2-based Zintl compounds are promising candidates for flexible thermoelectric materials, and their performance optimization strategies provides important references for the thermoelectric improvement of this group of materials. Hu *et al.*[57]

achieved a significant breakthrough in the thermoelectric performance of p-type Mg_3Sb_2-based materials via the synergistic regulation of electronic orbital alignment and hierarchical phonon scattering. Its core design involves two aspects: first, alloying at the Sb site by introducing Bi elements to regulate the overlap degree of electronic orbitals at the top of the valence band, increasing the effective carrier mass to 1.8 m_0 while maintaining high carrier mobility (~80 $cm^2 V^{-1} s^{-1}$), which significantly enhances the Seebeck coefficient (185 $\mu V K^{-1}$ at room temperature); second, constructing a three-level hierarchical structure of "point defects - grain boundaries - nano-domains", reducing the lattice thermal conductivity to 0.42 $W m^{-1} K^{-1}$ (300 K) via Sb/Bi atomic mass differences, grain refinement (particle size ~200 nm), and nano-domain boundary scattering. Benefiting from the above dual regulation, the thermoelectric figure of merit *ZT* of this p-type Mg_3Sb_2-Bi system reaches 1.5 at 573 K and 0.85 at room temperature, with an electrical conductivity of up to 320 $S cm^{-1}$ and a peak power factor of 108 $\mu W cm^{-1} K^{-2}$.

This strategy breaks the bottleneck of "incompatibility between high electrical conductivity and low thermal conductivity" in traditional IB_2-VIA group materials, demonstrating that the performance leap of p-type thermoelectric materials can be achieved via electronic structure regulation and multi-scale phonon scattering design. This provides new ideas for the p-type optimization and flexible device application of IB_2-VIA group nanomaterials[57].

VIB-VIA_2 thermoelectric materials mainly include MoS_2, WS_2, $MoSe_2$, and WSe_2[59-63]. First-principles (Density Functional Theory, DFT) calculations have demonstrated that monolayer transition-metal chalcogenides (TMDCs) exhibit excellent room-temperature thermoelectric performance, though their performance is still lower than that of traditional materials such as Bi_2Te_3 and Sb_2Te_3. Constructing heterostructures to enhance the thermoelectric performance of VIB-VIA_2 materials is a widely used strategy currently[59].

Liquid-phase exfoliation is a commonly used method for preparing VI-VI_2 nanomaterials. For example, Guo *et al.* used Li-ion intercalation in bulk MoS_2 in cyclohexane solvent to break the weak van der Waals forces between MoS_2 layers and exfoliated single-layer or few-layer MoS_2 via ultrasonication [Figure 3K][62]. However, MoS_2 prepared via ion-intercalation methods contains both the 1T metallic phase and 2H semiconducting phase; the poor conductivity of 2H-phase MoS_2 is unfavorable for optimizing the thermoelectric performance of MoS_2 materials. To further enhance thermoelectric performance, they modified the surface of MoS_2 nanosheets with an Au precursor solution to form Schottky contacts on the nanosheet surfaces, which act as carrier-transport channels and low-energy carrier-filtering barriers. By regulating the Au content, the electrical conductivity of Au- MoS_2 films increased from 88.7 $S cm^{-1}$ to 177.1 $S cm^{-1}$, and the energy-filtering effect promoted an increase in the Seebeck coefficient from 84.6 $\mu V K^{-1}$ to 96.9 $\mu V K^{-1}$; the optimal power factor was about 166.3 $\mu W cm^{-1} K^{-2}$. To further enhance thermoelectric performance, they compounded exfoliated MoS_2 nanosheets with CNTs and constructed porous structures via freeze-drying to reduce the thermal conductivity of the composite film; the thermal conductivity was as low as 19.3 m $W m^{-1} K^{-1}$. CNTs acted as conductive pathways to ensure carrier transport, so the corresponding *ZT* reached 0.17[64].

Organic thermoelectric materials

Types of conductive polymers

Conductive polymers generally contain conjugated π-bond structures with alternating single and double bonds. After chemical doping, π electrons can delocalize along the polymer backbone, resulting each carbon atom to have an unpaired π electron, thereby triggering charge transport and exhibiting conductive or semiconducting properties[65,66]. Based on the conduction mechanism, conductive polymers can be divided into composite-type and structural-type. Composite-type conductive polymers consist of a poorly

conductive polymer matrix, highly conductive fillers, and additives; their conductive function mainly depends on inorganic fillers. Common highly conductive fillers include conductive carbon materials and metal powders, for example. Structural-type conductive polymers are mostly conjugated polymers with highly delocalized electrons, which themselves can provide carriers and thus possess basic conductivity; after chemical or electrochemical doping, their electrical conductivity can be significantly improved and, even comparable to that of metals in some cases. Chemical doping or the introducing different valence states can alter the distribution of holes and electrons in conductive polymers, enabling precise regulation of their charge-transport properties. Chemical doping includes p-type and n-type doping, which essentially correspond to the oxidation or reduction processes of the conjugated polymer backbone: p-type doping corresponds to the oxidation of the conjugated chain, and n-type doping corresponds to the reduction of the conjugated chain. Among p-type conductive polymers, polyaniline (PANI), polypyrrole (PPy), and poly(3,4-ethylenedioxythiophene) (PEDOT) have the most application prospects. They exhibit high electrical conductivity, good stability, and simple synthesis, making them representative among conductive polymers.

Polyaniline

The thermoelectric performance of PANI mainly depends on its synthesis method and doping conditions. Currently, the structural formula of PANI generally adopts the benzoid-quinoid structural model, where the value of y reflects the redox state. When y = 0.5, the ratio of benzoid to quinoid structures in the molecular chain is 3:1 (a half-oxidized, half-reduced structure), referred to as emeraldine base PANI. In this state, PANI molecules can undergo a sudden transition from an insulating state to a conductive state via doping. When a protonic acid reacts with emeraldine base PANI, the amino groups are first protonated, and the positive charges carried by the protons transfer along the polymer backbone and become periodically distributed, altering the charge state of the molecular orbitals. The conduction mechanism of PANI mainly involves three models: the granular metal-island model, the electronic-conduction model, and the polaron-bipolaron model. The granular metal-island model posits that non-uniform doping creates metallic and non-metallic regions in the PANI chains, with metallic islands dispersed in an insulating matrix. The electron-hopping theory assumes that electrons in the PANI chains hop from reduced units to oxidized units to complete conduction. The polaron-bipolar on conversion model suggests that benzenoid bipolar facilitate charge transport along the molecular chains.

The electrical conductivity of PANI is significantly affected by the type of dopant acid. For example, Li *et al.* discussed the influence of HCl doping concentration on the thermoelectric performance of PANI within the temperature range of 303-423 K. Figure 4A and B show the synthesis mechanism of PANI and the Field Emission Scanning Electron Microscope (FESEM) image of HCl (1.0 M)-doped PANI powder. The results in Figure 4C show that with increasing HCl doping concentration, the electrical conductivity of PANI first increases and then decreases[67]. Yao *et al.* synthesized fibrous PANI powder using camphor sulfonic acid (CSA) as the dopant and m-cresol as the solvent. Compared with amorphous PANI, PANI with such micro-nano structures have a more ordered chain arrangement; the templating effect of CSA promotes the growth of PANI toward a more crystalline orientation during synthesis, consequently enhancing both the electrical conductivity and Seebeck coefficient of PANI/CSA, with the power factor approximately 20 times that of PANI synthesized without CSA doping. Subsequently, the same research group successfully prepared PANI films with different packing states by simply adjusting the m-cresol solvent content, using CSA as the dopant acid[68,69].

The intrinsic electrical conductivity of PANI is relatively low. Although the thermoelectric performance of pure PANI systems has been significantly improved in recent years, it is still difficult to meet the requirements of practical applications. Thus, researchers have conducted extensive studies on PANI-based composites and hybrid materials. In the preparation of such materials, commonly used fillers can be divided

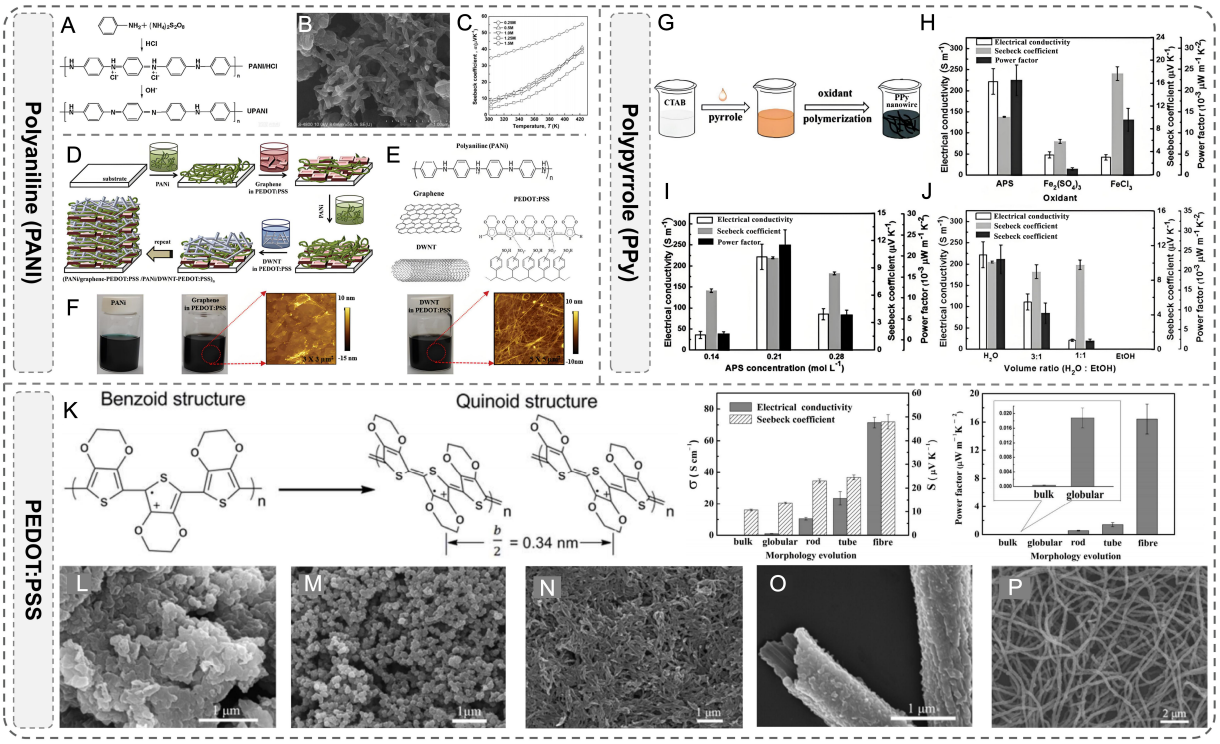

Figure 4. (A) Synthesis mechanism of PANI, (B) FESEM image of HCl (1.0 M) doped PANI powder and (C) The temperature dependence of the Seebeck coefficient of various HCl-doped PANI. (A-C) Reproduced with permission[67]. Copyright 2010, Elsevier; (D) Schematic of the layer-by-layer deposition process; (E) The structure of thermoelectric film components used; (F) Images of aqueous PANI solution, and graphene and DWCNT stabilized by PEDOT:PSS, in water; (D-F) Reproduced with permission[70]. Copyright 2016, WILEY-VCH; (G) Schematic illustration showing the preparation process for the PPy nanostructures by chemical oxidation polymerization; (H) Thermoelectric performance of electrical conductivity, Seebeck coefficient and power factor for PPy prepared with different oxidants; (I) Thermoelectric performance of electrical conductivity, Seebeck coefficient and power factor for PPy nanowires prepared at different APS concentrations; (J) Thermoelectric performance of electrical conductivity, Seebeck coefficient and power factor for the PPy samples prepared in various reaction media; (G-J) Reproduced with permission[71]. Copyright 2017, Royal Society of Chemistry; (K) Schematic presentation of the PEDOT benzoid structure, the ordered quinoid structure in bulk and nanostructured PEDOT samples and Thermoelectric performance of bulk PEDOT and PEDOT nanostructures; FESEM images of (L) bulk PEDOT power and PEDOT nanostructures of (M) globular nanoparticles, (N) nanorods or ellipsoidal nanoparticles, (O) nanotubes and (P) nanofibers; (K-P) Reproduced with permission[77]. Copyright 2015, Royal Society of Chemistry. PANI: Polyaniline; PEDOT: poly(3,4-ethylenedioxythiophene); PSS: polystyrene sulfonate; PPy: polypyrrole; APS: ammonium persulfate; FESEM: field emission scanning electron microscope; DWCNT: double-walled carbon nanotube; DWNT: double-walled nanotube.

into two categories: one includes highly conductive inorganic materials such as Te, Bi_2Te_3, and PbTe; the other includes carbon materials such as graphene, CNTs, and graphite. Incorporating these fillers into the PANI matrix enables the preparation of binary or multicomponent composites. Layer-by-layer self-assembly is also an effective approach to enhance the thermoelectric performance of PANI-based composites; for example, PANI/graphene-PEDOT:PSS (polystyrene sulfonate)/PANI/DWCNT (double-walled carbon nanotube)-PEDOT:PSS composite films can be prepared via layer-by-layer assembly, as shown in Figure 4D-F[70].

Polypyrrole

PPy not only exhibits good stability in air but also achieves relatively high electrical conductivity at suitable doping levels. However, research on the thermoelectric performance of PPy and its composites has been relatively limited in recent years, and its thermoelectric performance still cannot compete with that of mainstream conductive polymer thermoelectric materials such as PANI and PEDOT.

In the synthesis of conductive polymers, carrier mobility is a key indicator affecting their conductive performance and application potential, and constructing low-dimensional nanostructures is an effective means to enhance this performance. Low-dimensional morphologies such as nanowires, nanorods, nanofibers, and nanotubes can significantly shorten carrier-transport paths, reduce charge scattering and recombination during transport, and increase specific surface area to construct more efficient charge-transport channels, thereby significantly improving carrier mobility in conductive polymers[70,71]. As a conductive polymer with good conductivity, environmental stability, and ease of preparation, PPy is often fabricated into micro-nano structures with the soft-template method as the first choice. This method features simple operation, precise morphology control, and low cost, and has become the most widely used technique currently. Via electrostatic interactions, hydrophobic interactions, or π-π stacking between soft templates and PPy monomers, the monomers can be guided to polymerize directionally into the desired micro-nano structures. Common soft templates include anionic surfactants such as sodium dodecyl sulfate (SDS) and sodium alkyl sulfonate (SAS), as well as cationic surfactants such as cetyltrimethylammonium bromide (CTAB), which form micelles via self-assembly to provide template spaces for polymerization. Organic dyes such as acid red B and methyl orange (MO) can act as both templates and dopants, simultaneously optimizing the morphology and conductivity of PPy. Cyclodextrins, with their unique cavity structures, can realize precise regulation of PPy micro-nano structures via host-guest recognition.

For example, Liang *et al.* used CTAB as a template agent and studied the effects of preparation conditions such as oxidant type and concentration, reaction medium, and reaction time on the nanostructure and thermoelectric performance of PPy, as shown in Figure 4G-J. The results showed that PPy nanowires exhibited the best thermoelectric performance. After further optimizing the ammonium persulfate concentration and reaction time, the maximum power factor of PPy reached $(22.6 \pm 3.6) \times 10^{-3}$ μW m^{-1} K^{-2}[71].

In addition to the soft-template method, the light-controlled precise regulation strategy provides an innovative path for the designable preparation of PPy conductive patterns. Zhao *et al.* developed a light-controlled Fe^{3+} initiator concentration regulation technology, which has achieved arbitrarily designed PPy conductive patterns in polyvinyl alcohol/sodium alginate (PVA/SA) semi-interpenetrating network hydrogels[72]. Its core mechanism is as follows: the reduction degree of Fe^{3+} ions coordinated with carboxylate groups is precisely regulated via ultraviolet light irradiation time; after Fe^{3+} is partially reduced to Fe^{2+}, only the residual Fe^{3+} acts as an initiator to trigger the controllable polymerization of pyrrole monomers in designated areas, thereby forming target conductive patterns. This process has been verified by Fourier transform infrared spectroscopy (FTIR), X-ray photoelectron spectroscopy (XPS), and scanning electron microscopy (SEM). The electrical conductivity of the patterned PPy hydrogel can reach up to 128 S·cm^{-1}, and its pattern resolution is superior to 50 μm, exhibiting excellent conductive uniformity and structural stability; it can not only be used for flexible intelligent conductive circuits but also realize the information storage function through pattern encryption. This light-controlled strategy does not require complex template removal steps, solving the problem of insufficient flexibility in pattern design of traditional soft-template methods; meanwhile, it expands the application potential of PPy-based materials in thermoelectric-information integrated devices, providing new ideas for the functional integration of flexible thermoelectric materials[72].

Incorporating highly conductive fillers such as CNTs and graphene into the PPy matrix can effectively enhance the electrical conductivity of PPy composites. For example, Wang *et al.*[73] first prepared MWCNT/PPy nanocomposites with core-shell structures using p-toluene sulfonic acid as the dopant. Subsequently, the same research group further investigated the thermoelectric performance of MWCNT/PPy nanocomposites by comparing *in-situ* polymerization and solution-mixing methods. Although the thermoelectric performance of PPy-based composites is still not optimal, related studies have demonstrated

their application potential in fields such as temperature sensing[74,75].

PEDOT

Besides PPy-based composites, PEDOT is a derivative of polythiophene; Bayer developed PEDOT to solve the poor solubility of poly(3-hexylthiophene) (P3HT)[76]. The nanostructures, thermoelectric performance, and related FESEM images of PEDOT are shown in Figure 4K-P[77]. To further enhance the processability of PEDOT, researchers introduced the water-soluble electrolyte PSS into PEDOT chains to obtain a PEDOT:PSS dispersion. The PEDOT: PSS dispersion exhibits excellent thermoelectric and optoelectronic properties, and its mature commercial products provide great convenience for studies on PEDOT-based systems in the fields of energy materials and flexible electronics.

Similar to other conductive polymers, the thermoelectric performance of PEDOT:PSS is closely related to core factors such as degree of polymerization, crystallinity, doping level, and chain-packing mode. Based on this correlation, targeted optimization of these factors can effectively enhance the thermoelectric performance of PEDOT:PSS. For example, Bubnova *et al.*[78] prepared PEDOT:Tos via vapor-phase polymerization and treated it with tetrakis(dimethylamino)ethylene (TDAE) vapor. When the oxidation degree of PEDOT was 22%, the maximum power factor reached 324 μW cm^{-1} K^{-2}.

The electrical conductivity and Seebeck coefficient of PEDOT:PSS are not only determined by its oxidation degree but also significantly affected by molecular-chain conformation and morphology. Among various optimization methods, secondary-doping treatments are the most widely used. In the secondary doping of PEDOT:PSS, commonly used reagents include high-dielectric-constant polar solvents such as dimethyl sulfoxide (DMSO) and ethylene glycol (EG); co-solvent systems composed of low-polarity solvents and water, such as ethanol/water, acetonitrile/water, and N,N-dimethylformamide (DMF)/water; acids and ionic liquids are also often used as secondary dopants. For example, Kim *et al.*[79] found that polar solvents such as DMSO and EG can counteract the screening effect between carriers and ions and reduce the Coulombic interaction between charges, but this method does not change the doping level of PEDOT:PSS, so it has little effect on the Seebeck coefficient. Ouyang *et al.*[80] investigated the influence of the number of polar groups in solvents (EG, DMSO, 2-nitroethanol, and 1-methyl-2-pyrrolidone) on the electrical conductivity of PEDOT:PSS. The interaction among dipoles causes the molecular conformation of PEDOT to change from a coiled benzenoid structure to a linear quinoid structure, thereby enhancing carrier mobility. Jönsson *et al.*[81] suggested that polar solvents can promote the formation of PEDOT crystallites and enhance the ordered arrangement and crystallinity of conductive PEDOT chains.

Additionally, the use of ionic liquids to enhance the thermoelectric performance of PEDOT systems has also achieved certain progress. For example, Kee *et al.*[82] investigated the effects of [EMIM]X ionic liquids-where EMIM is 1-ethyl-3-methylimidazolium cation and X is Cl^-, ethyl sulfate (ES), tricyanomethanide (TCM), or tetracyanoborate (TCB) - on the thermoelectric performance of PEDOT:PSS. The electrical conductivity of PEDOT:PSS is closely related to the molecular weight of PEDOT. Fan *et al.*[83] compared various parameters of two commercial PEDOT:PSS products, Clevios P and Clevios PH1000, in detail. Petsagkourakis *et al.*[84] also theoretically demonstrated that longer molecular chains within a certain range are beneficial for enhancing carrier transport in conductive polymers. Due to the presence of PSS, PEDOT:PSS can also transport ions and serves as an ion/electron mixed conductor; under high-humidity conditions, the Seebeck coefficient of PEDOT:PSS is enhanced due to ionic thermoelectric effects[85]. Wang *et al.*[86] studied PEDOT:PSS and PEDOT:Tos systems and found that under low-humidity conditions, the Seebeck coefficients of the two are basically the same; as humidity increases, the Seebeck coefficient of PEDOT:PSS increases significantly. Notably, although increasing humidity significantly enhances the Seebeck coefficient, the stability of this effect is low; over time, the electronic Seebeck effect still becomes dominant.

Besides the above optimization methods, the preparation of PEDOT-based composites has also been extensively investigated. However, the microscopic mechanism changes during the composite and hybrid processes remain unclear, and the corresponding theoretical framework needs to be further in-depth studied.

Interface compatibility mechanisms of inorganic-organic composites

Inorganic-organic composites (e.g., CNT/PEDOT:PSS, MoS_2/CNTs, Bi_2Te_3/PEDOT:PSS) integrate the high thermoelectric performance of inorganic materials and the flexibility of organic polymers[87,88]. However, interface compatibility issues (e.g., charge transport barriers, weak interface binding) limit their performance optimization[89]. Energy level mismatch between inorganic and organic phases forms a Schottky barrier. For example, the work function of CNTs is ~4.5 eV, while that of PEDOT:PSS is ~5.0 eV, resulting in a 0.5 eV Schottky barrier at the interface, which hinders carrier transport[64,73]. Weak physical adsorption (e.g., van der Waals forces between MoS_2 and CNTs[62,64]) leads to poor interface binding, causing phase separation under mechanical deformation or environmental stimulation. Gold (Au) nanoparticles are modified on MoS_2 surfaces to form ohmic contacts, eliminating charge transport barriers. Porous structures constructed via freeze-drying balance phonon scattering and thermal gradient maintenance, increasing the *ZT* value to 0.17[62,64]. Additionally, discontinuous interface structures enhance phonon scattering, which helps reduce thermal conductivity but may excessively suppress heat transfer, affecting the establishment of effective temperature gradients[64,90]. These regulatory strategies provide effective solutions for enhancing the interface compatibility of inorganic-organic composites, laying a foundation for the development of high-performance flexible thermoelectric materials[91].

Large-scale fabrication bottlenecks

While significant progress has been made in the preparation of flexible thermoelectric materials (e.g., carbon nanomaterials, chalcogenides, and conducting polymers), their large-scale production (e.g., roll-to-roll coating, mass spinning) still faces technical bottlenecks such as uniformity control, cost reduction, and process compatibility. For 1D thermoelectric fibers (e.g., CNT yarns, SnSe fibers), uneven dispersion of thermoelectric components during spinning results in inconsistent performance among batches[92]. For 2D films [e.g., PEDOT:PSS, Bi_2Te_3/polyvinylidene fluoride (PVDF) composite films], thickness fluctuation (typically ±10%) is prone to occur during roll-to-roll coating, affecting the stability of device performance[93]. High-purity carbon nanomaterials (e.g., SWCNTs) and chalcogenide nanocrystals (e.g., Bi_2Te_3, Ag_2Se) have high raw material costs. Complex preparation processes (e.g., solvothermal synthesis, ion intercalation) further increase production costs[54,62,78]. Traditional inorganic thermoelectric materials (e.g., Bi_2Te_3, Sb_2Te_3) are brittle, making them difficult to integrate with flexible substrate manufacturing processes (e.g., weaving, coating)[8,9].

Environmental durability

Environmental durability (e.g., resistance to humidity, sweat, and oxygen) is a key bottleneck limiting the practical application of flexible thermoelectric materials, and system-level performance failures (e.g., cracking, interfacial delamination, performance degradation) induced by these factors under long-term wearable mechanical deformation are critical practical challenges. This study conducted direct and critical comparisons of the environmental durability of inorganic, organic, and inorganic-organic composite thermoelectric material systems under a unified wearable test framework, systematically analyze their failure and success mechanisms in wearable application scenarios, and proposed targeted optimization strategies for each material system accordingly. The durability test environment is as follows, Temperature = 25 °C, humidity = 60%-80%, sweat simulant = 0.9% NaCl solution, aging cycle = 30 days (continuous immersion for organic materials, cyclic exposure for inorganic/composite materials).

For inorganic materials, chalcogenide components (e.g., Te in Bi_2Te_3, Se in Ag_2Se) are prone to oxidation in humid and sweat environments, forming brittle oxide layers that reduce interface bonding strength, thereby impairing mechanical compliance. Oxidation-induced brittleness easily causes cracking under long-term wearable bending/twisting, and oxide accumulation further leads to interfacial delamination at material-substrate interfaces. This is a core failure factor for inorganic materials in long-term wearable use, with controversial oxidation kinetic pathways reported in literature. This strategy succeeds in mitigating oxidation but cannot fundamentally solve the brittleness issue of inorganic materials under wearable deformation.

For organic materials, water molecules penetrate the polymer matrix, leading to the loss of protonic dopants (e.g., HCl in PANI, PSS^- in PEDOT:PSS); meanwhile, chemical bonds in the polymer backbone (e.g., ether bonds in PEDOT) undergo hydrolysis or oxidation, reducing the degree of conjugation and charge mobility. Sweat and humidity cause continuous performance degradation, and excessive matrix swelling under hydration may trigger interfacial delamination with electrode layers[67,70]. The literature reports inconsistent conclusions on the dopant retention efficiency of different organic systems under sweat immersion. The literature also reports contradictory results on the trade-off between crosslinking degree, electrical conductivity, and flexibility for wearable use[94].

Finally, for inorganic-organic composites, water molecules weaken the weak interfacial interactions (e.g., van der Waals forces, hydrogen bonds) between inorganic fillers and organic matrices, leading to filler detachment and phase separation, which reduces charge transport efficiency and structural integrity[95]. Filler detachment easily causes micro-cracking in the bulk phase, and interfacial weakening triggers local delamination under repeated mechanical deformation[64,73]. This hybrid system achieves a performance balance for wearability, making it the most promising strategy among the three material systems. This dual optimization strategy succeeds in addressing both interfacial failure and performance imbalance, with no contradictory results reported in wearable-relevant studies[96-98].

FLEXIBLE WEARABLE THERMOELECTRIC GENERATORS

f-TEGs are devices that capable of converting thermal energy into electrical energy, with broad application prospects. In particular, they provide a feasible approach for energy harvesting in wearable electronic devices and smart textiles. According to differences in structural dimensionality and working principles, f-TEGs can generally be classified into three categories: 1D fiber materials, 2D film materials, and 3D bulk materials. Each type of structure has its own advantages and applicable fields; selecting appropriate materials and structural designs is crucial for enhancing the thermoelectric performance of f-TEGs.

Notably, the performance evaluation of f-TEGs for wearable scenarios cannot be limited to basic thermoelectric parameters (e.g., ZT, S, σ, κ) alone. By synthesizing existing studies, we summarize a multi-dimensional comprehensive performance evaluation system[99-102].

Bending cycle count (test condition: bending radius R = 5 mm) and performance attenuation rate have been widely reported in existing research - for example, fiber-based devices can withstand more than 1,000 bending cycles with a ZT retention rate of more than 85%[102], while bulk-based devices typically endure 300-500 cycles with an attenuation of less than 20%.

Tensile strain tolerance threshold, with reported values of not less than 20% for joint-worn film devices[99] and not less than 50% for textile-integrated fiber devices[101], reflecting adaptation to different wearable deformation scenarios. Other core evaluation criteria include biocompatibility (most reported wearable materials meet in vitro cytotoxicity standards with cell viability not less than 90%)[103], substrate softness

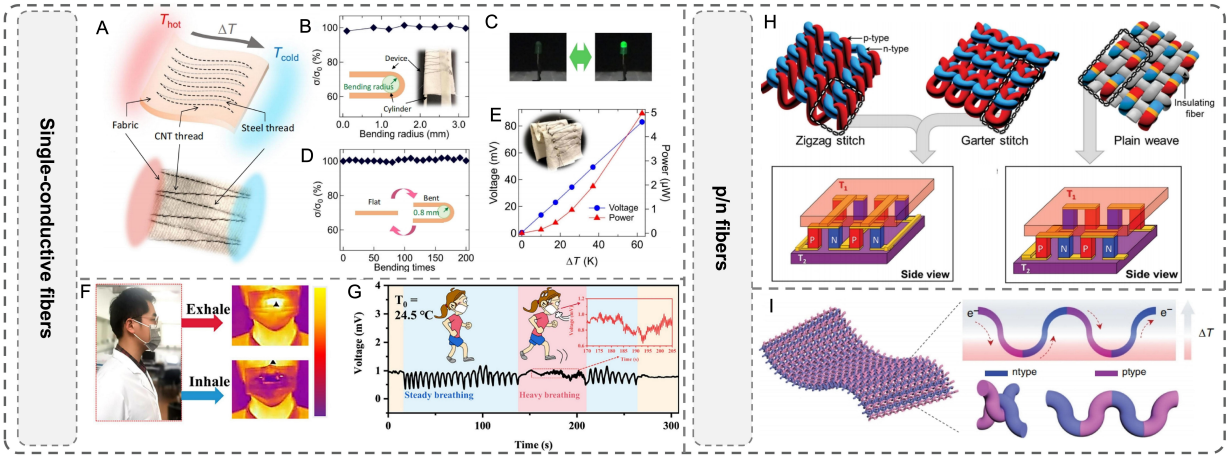

Figure 5. (A-E) Morphology and performance testing of TE fabrics based on p-type CNTs yarns. (A-E) Reproduced with permission[104]. Copyright 2021 Springer Nature; (F and G) wearable demonstration of TEGs in wristbands and masks. (F and G) Reproduced with permission[106]. Copyright 2022, Elsevier; (H) Schematic diagram of weaving structure of various TE fabrics and corresponding TEG models. Reproduced with permission; (H) Reproduced with permission[102]. Copyright 2016, WILEY-VCH; (I) schematic diagram of plain-weave TE fabric. (I) Reproduced with permission[3]. Copyright 2020 Springer Nature. CNTs: Carbon nanotubes; TE: thermoelectric; TEGs: thermoelectric generators.

(modulus ≤ 1 GPa to avoid skin irritation)[99], and breathability (fiber/textile devices typically exhibit air permeability ≥ 500 mm/s)[102], all of which are core evaluation criteria verified in practical wearable studies. This integrated evaluation system reflects the consensus of current research on the performance of wearable f-TEGs, linking the properties of materials/devices with actual application demands.

One-dimensional fiber-based wearable thermoelectric generators

Fibers can be woven into fabrics with various structures and then further processed into garments, serving as important microelectronic carriers in smart clothing. Among them, designing and preparing thermoelectric fibers, weaving them into fabrics and garments, and then harvesting body heat to power wearable electronics is an effective solution to the energy supply problem of smart clothing and has enormous market potential. According to differences in weaving structures, wearable thermoelectric devices based on fiber materials can be classified into two types: the first type is wearable thermoelectric devices based on single-conductive fibers, and the second type is wearable thermoelectric devices based on p/n-segmented fibers.

Wearable thermoelectric devices based on single-conductive fibers

In single-conductive fibers, the majority carriers are uniformly distributed and of a single type (only electrons or only holes). When such fibers are used for thermal energy harvesting, they can only form a temperature gradient in one direction. To establish an effective temperature difference, thermoelectric devices based on single-conductive fibers must satisfy specific layouts: one end is attached to a thermal source (such as human skin), and the other end is exposed to the environment to dissipate heat via air. Komatsu *et al.* at Rice University sewed single-conductive CNT fibers into ordinary fabrics and used stainless-steel wires as electrodes to connect CNT fibers in series [Figure 5A-E][104]. When the temperature difference between the two ends of the fabric reached 60 K, the open-circuit voltage and output power of the device were 83 mV and 5.0 μW, respectively[105]. He *et al.* combined hybrid fibers prepared by wet spinning with masks to obtain fabric-based thermoelectric devices that can harvest thermal energy from the exhaled breath from the mouth and the heat from the wrist [Figure 5F and G][106].

Compared with carbon and organic materials, fibers based on inorganic semiconductors have higher thermoelectric performance; thus, the fabric-based thermoelectric devices woven from them can output more electrical energy under the same temperature difference[107]. Zhang *et al.* at Nanyang Technological

University wove single-crystal SnSe fibers prepared by hot-drawing into two-dimensional fabrics to create wearable thermoelectric textiles[92]. When one end is attached to the skin and the other end is exposed to the environment, the fabric can output approximately 30 mV in an environment of 25 °C. In addition, they also prepared fabric devices based on Bi_2Se_3 fibers and $Bi_{0.5}Sb_{1.5}Te_3$ fibers and studied their cooling capability under different currents and environments. When a current of 3.5 mA was applied, the temperature at the cold end of the device decreased by 4.9 °C, indicating that it can be used for managing human thermal comfort[108].

Wearable thermoelectric devices based on p/n fibers

Thermoelectric devices based on single-conductive thermoelectric fibers can only form a temperature gradient in the in-plane direction of the fibers, which imposes significant limitations on body-heat conversion efficiency and wearing comfort. In contrast, p/n-structured thermoelectric fibers can be directly woven into thermoelectric fabrics via coil structures; by utilizing the natural undulations of thermoelectric fibers within fabrics, heat conversion along the direction of the human-body temperature gradient can be achieved. Lee *et al.* at the University of Texas at Dallas studied thermoelectric-fabric structures constructed by different knitting methods and their working models [Figure 5H][102]. To construct thermoelectric fabrics entirely from p/n fibers, Ding *et al.* built plain-weave thermoelectric fabrics based on p-type and n-type CNT thermoelectric fibers [Figure 5I][3]. In both the warp and weft directions, p/n fibers alternately contact each other to establish a thermally parallel structure; the waterproof coating on the fiber surface prevents short circuits caused by fabric deformation. In this work, the plain-weave thermoelectric fabric composed of 264 pairs of thermoelectric legs output an open-circuit voltage of approximately 20 mV and a power of about 100 pW under a temperature difference of 20 K. In addition, the thermoelectric fabric can also be used for body-temperature and photothermal sensing to monitor human motion and light-source information.

Different coil interlocking modes also affect the overall structure of thermoelectric fabrics and thereby influence thermal energy conversion efficiency. Sun *et al.* constructed various thermoelectric fabrics based on different coil interlocking modes and investigated their electrical output performance under 2D and 3D deformation[101]. In 3D-structured thermoelectric fabrics, the angle between the yarn length direction in coils and the human-body temperature gradient is smaller, which is more conducive to maintaining a large temperature difference; the output voltage of such fabrics is 24 times that of 2D-structured thermoelectric fabrics. Furthermore, the 3D structure endows the fabric with excellent stretchability, thereby enhancing wearing comfort[109].

Two-dimensional film materials

Due to their excellent flexibility, flexible film materials are highly suitable for fabricating wearable thermoelectric devices. According to different construction methods, the structures of film-based wearable thermoelectric devices are mainly classified into planar structures and helical structures.

Planar-structure wearable thermoelectric devices

In planar-structure wearable thermoelectric devices, thermoelectric films serve as the main component for thermoelectric conversion and rely on the substrate to establish a temperature gradient that regulates heat transfer. For example, Guo *et al.* used ordinary fabrics as supporting substrates and embedded gold-molybdenum disulfide (Au-MoS_2) films on both sides of the fabrics to prepare flexible thermoelectric wristbands[62]. When worn on the human arm, the side close to the skin acts as the hot end, and the side exposed to the environment acts as the cold end; body heat is transferred from the hot end to the cold end, establishing a temperature difference between the two ends of the thermoelectric wristband. Under a temperature difference of 5 K, the thermoelectric wristband can output an open-circuit voltage of approximately 2.4 mV and still operate stably after more than 500 bending cycles.

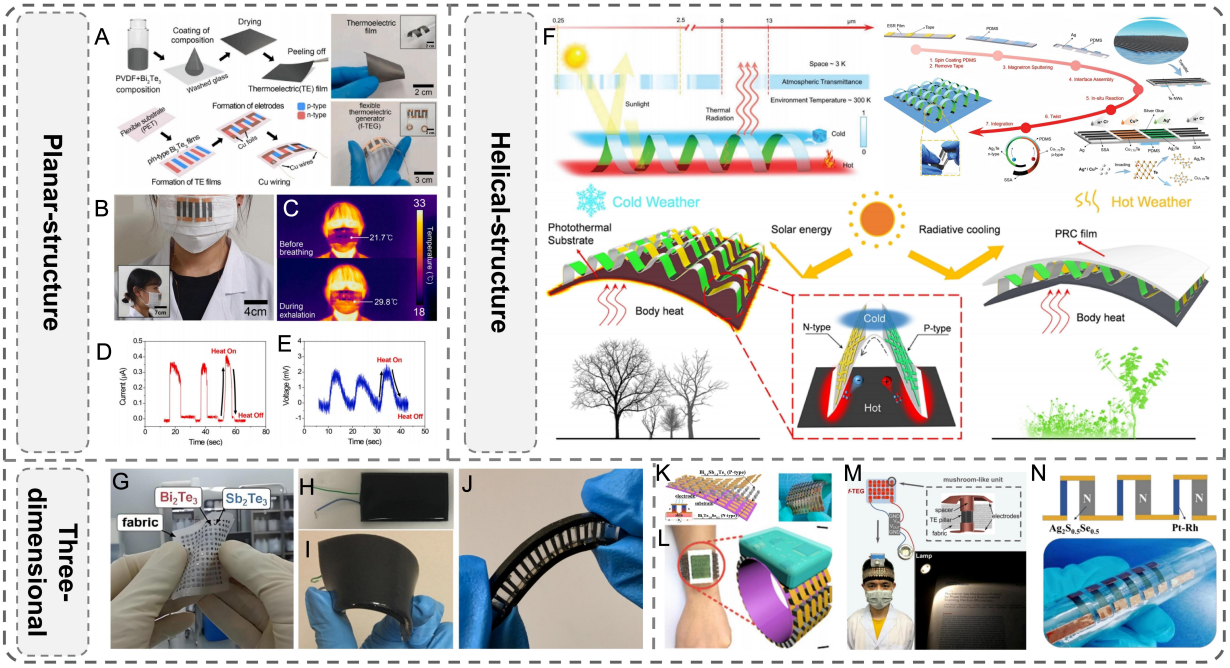

Figure 6. (A) Schematic illustrations of Bi_2Te_3/PVDF thermoelectric (TE) film fabrication and multicouple flexible thermoelectric generator (f-TEG) fabrication; (Insets) Photographs of the bent Bi_2Te_3/PVDF TE film (rolled on a plastic cylinder) and the bent/completed f-TEG; (B) Mask photos, (C) Infrared thermal imaging (D) Output current signals and (E) output voltage signals from the human body heat during breathing. (A-E) Reproduced with permission[100]. Copyright 2022, Elsevier; (F) Preparation process of helical TEGs; (F)Reproduced with permission[93]. Copyright 2022, WILEY-VCH. And schematic diagram of the structure of a wave-shaped TEG with radiative cooling performance; (F) Reproduced with permission[114]. Copyright 2022, American Chemical Society. Flexible thermoelectric generators based on three-dimensional bulk material; (G) f-TEGs with bots of thermal legs on glass fabric. (G) Reproduced with permission[119]. Copyright 2014, Royal Society of Chemistry; (H-J) f-TEGs with bulk materials as legs and liquid metals as connections. (H-J) Reproduced with permission[120]. Copyright 2020, Elsevier; (K and L) f-TEGs with bulk materials and a polyimide substrate and Schematic view of the self-powered wearable bracelet integrating an f-TEG. (K and L) Reproduced with permission[121]. Copyright 2020, Elsevier; (M) f-TEG with mushroom-shaped modules powering a lamp. (M) Reproduced with permission[122]. Copyright 2022, Elsevier; (N) f-TEG with bulk and fiber materials; (N) Reproduced with permission[123]. Copyright 2019, Royal Society of Chemistry. PVDF: Polyvinylidene fluoride; TEG: thermoelectric generator; PDMS: polydimethylsiloxane; SSA: selective solar absorption; PRC: passive radiative cooling; PVDF: polyvinylidene fluoride.

Figure 6A shows a schematic illustration of the fabrication procedure for the free-standing thermoelectric film using p-type and n-type Bi_2Te_3 powders and PVDF. Na *et al.* at Kyungpook National University in Korea constructed planar-structure thermoelectric arrays on the surface of masks to harvest thermal energy from human residual heat [Figure 6B-E][100]. When the device is placed at the mouth, one end acts as the hot end to harvest thermal energy from the heat released during breathing. Under a temperature difference of approximately 8 K between the two ends, the open-circuit voltage and output current of the device are 2.3 mV and 0.38 μA, respectively.

The practical application potential of planar-structured wearable thermoelectric devices can be further verified by superhydrophobic surface design and encapsulation-free stability data[103,110]. This study indicates that by constructing a micro-nano scale superhydrophobic surface (water contact angle not less than 152°), the erosion of the device interface by human sweat and environmental moisture can be effectively isolated. Meanwhile, the thin-film device developed in this study, without an additional encapsulation layer, maintains a thermoelectric conversion efficiency retention rate of 96.5% and an open-circuit voltage attenuation of only 2.8% after 1000 cyclic bending cycles (bending radius of 5 mm); after long-term exposure to a room temperature environment (25 °C, humidity 40%-80%) for 30 days, the power factor still retains 94.2% of its initial value[111]. Collectively, this finding demonstrates that the superhydrophobic surface design effectively addresses the critical challenges of antifouling and moisture resistance for wearable devices, while

the exceptional encapsulation-free stability simplifies the device fabrication process and reduces associated costs. Together, they confirm the durability and adaptability of planar-structured devices in human wearing scenarios, which can meet daily usage needs without complex encapsulation, further consolidating their practical application value[38].

The practical wearability of planar-structured devices depends not only on thermoelectric conversion efficiency but also on performance stability under mechanical deformations such as repeated bending and stretching. The flexible piezo-ionic skin developed by Wang *et al.* provides an innovative solution for enhancing the stability of planar-structured devices through the synergistic design of dynamic hard domains and mechanosensitive ionic channels[99]. Its core design lies in introducing carboxyl-functionalized groups into the dynamic hard domains of the poly(urethane-urea) matrix: on one hand, a high-strength network is constructed through multiple non-covalent interactions; on the other hand, the electrostatic interaction between carboxyl groups and ionic liquids forms dynamically restricted ionic channels.

This structure endows the material with ultra-high fracture energy (211.27 kJ/m^2, more than 123.5 times that of human skin), excellent self-healing ability (self-healing efficiency of 96.40% within 24 h at room temperature), and high-pressure sensitivity (7.03 kPa^{-1}). Notably, after 1000 cyclic bending cycles (bending radius of 5 mm), the ionic transport efficiency of the piezo-ionic skin only degrades by 3.2% without obvious cracks; even when subjected to mechanical cutting, it can achieve functional recovery through dynamic bond recombination[112]. This design strategy breaks the bottleneck of "incompatibility between high flexibility and high toughness" in traditional planar devices, proving that regulating micro-stress distribution via dynamic hard domains and ensuring signal transmission stability through ionic channels can significantly enhance the durability of planar-structured devices in scenarios such as human joint movement and daily wearing friction. For thermoelectric planar devices, this structural optimization idea can be directly adopted - integrating the dynamic hard domain design into the substrate or functional layer not only retains the thinning advantage of planar structures but also enhances crack resistance and self-healing ability, further expanding the wearable adaptation scenarios of planar thermoelectric devices[99].

Helical-structure wearable thermoelectric devices

Helical-structured thermoelectric devices can also harvest thermal energy along the temperature-gradient direction and thus can be directly applied in wearable thermoelectric fields. Chen *et al.* partially introduced Ag^+ and Cu^+ onto self-assembled Te-nanowire films to prepare thermoelectric ribbons with alternating n-type Ag_2Te and p-type $Cu_{1.75}Te$ segments, twisted them into helical arrays, and fixed them onto substrates to form wearable thermoelectric devices [Figure 6F][93]. Pre-stretching processes can also be used to prepare helical-structured wearable thermoelectric devices. Nan *et al.* first interconnected p-type and n-type silicon chips into planar serpentine ribbons, encapsulated them with polymer coatings, embedded them into pre-stretched elastomer substrates, and finally formed helical-structured flexible thermoelectric devices after curing and releasing[113]. Such helical-structure flexible devices can conformally attach to multiple parts of the human body to realize real-time conversion of human residual heat. Chen *et al.* further constructed a novel Janus helical structure by bending alternating p-type $Cu_{1.75}Te$ and n-type Ag_2Te segments into Janus shapes and fixing them to photothermal films at the hot ends [Figure 6F][114].

Notably, the core advantage of helical-structured devices lies in adapting to dynamic human wearable scenarios through configurational deformation, but the tensile tolerance and signal response sensitivity of the device still depend on the performance optimization of the functional layer material. The MXene-based composite hydrogel developed by Lu *et al.*[115] provides key technical support for enhancing the mechanical stability and sensitivity of helical-structured devices. Its core preparation process is: using MXene ($Ti_3C_2T_x$)

as the conductive functional phase, covalently crosslinking with polyacrylamide (PAM) hydrogel through the free radical polymerization, and introducing a dynamic hydrogen bond network coordinated by Fe^{3+}-carboxyl groups to construct a "conductive network-dynamic crosslinking" dual-structure system. The composite hydrogel exhibits excellent mechanical properties: the tensile breaking strain reaches 1500%, the compressive strain tolerance exceeds 80%, and the mechanical property attenuation is only 4.3% after 100 cyclic stretches (500% strain); its pressure sensitivity is as high as 7.03 kPa^{-1} (in the range of 0-10 kPa), the response time is as short as 20 ms, and it has room-temperature self-healing ability (92.1% self-healing efficiency within 24 h)[115, 116].

Combining this composite process with helical-structured design can significantly enhance the wearable adaptability of the device: the high conductivity of MXene ensures thermoelectric conversion efficiency, the dynamic crosslinking network mitigates stress concentration during helical deformation, preventing electrode detachment or functional layer cracking; the high sensitivity enables the helical device to accurately capture thermoelectric signal changes caused by tiny human deformations (such as joint movement and breathing fluctuations). This technical path breaks the limitation that traditional helical-structured devices "cannot simultaneously achieve high stretchability and high stability", providing a direct reference for the mechanical performance optimization and sensitivity improvement of helical-structured wearable thermoelectric devices, which is particularly suitable for wearable scenarios requiring frequent deformation (such as the wrist and elbow joints).

Three-dimensional bulk materials

The greatest advantage of 3D bulk materials in f-TEGs lies in their higher thermoelectric performance and stability. To maintain high flexibility when designing f-TEGs, the size of these 3D bulk units is usually very small, and it is often necessary to appropriately design flexible substrates and fillers[117,118]. Figure 6G shows a 40 mm × 40 mm glass fabric device with Bi_2Te_3 and Sb_2Te_3 as thermoelectric legs[119]. 133 Figure 6H-J compares the power densities of Bi_2Te_3/Sb_2Te_3 devices using Al_2O_3 and flexible glass fibers as substrates under different ΔT values. The device with a flexible glass-fabric substrate achieved a high output power density of 35 W m^{-2} at a temperature difference of 50 K, indicating great application potential[119]. In addition to using glass fabrics as flexible substrates and PDMS as filling materials, some studies focus on designing high-pore-size elastomer encapsulation for f-TEGs and using liquid metals as connecting electrodes[120]. Figure 6K shows images of f-TEGs composed of bulk $Bi_{0.5}Sb_{1.5}Te_3$ and $Bi_2Se_{0.3}Te_{2.7}$ legs, where p-type and n-type legs are connected by graphene-nanosheet/eutectic gallium-indium liquid metals, and the encapsulation layer is elastomer PDMS. The advantage of liquid-metal connections is that they can enhance the stretchability between thermoelectric legs and reduce resistance caused by stretching. Another method to enhance the performance of miniaturized bulk-based f-TEGs is to decouple the factors affecting overall performance. A typical example is an f-TEG composed of p-type $Bi_{0.5}Sb_{1.5}Te_3$ and n-type $Bi_2Te_{2.8}Se_{0.2}$ micro-bulk legs and a polyimide flexible substrate, as shown in Figure 6L[121]. This device optimizes power density, material consumption, and power matching with wearable electronic devices and can be worn on the wrist as a wearable sensing system. Figure 6M shows an f-TEG composed of mushroom-shaped modules powering a lamp[122]. Figure 6N shows the structure and photographs of an f-TEG composed of bulk and fiber materials, where Se-doped Ag_2S acts as n-type legs and Pt-Ru wires act as p-type legs; the inset shows the ductility of $Ag_2S_{0.5}Se_{0.5}$[123].

Besides 3D bulk materials, aerogels also show great application potential in flexible thermoelectric devices due to their extremely low thermal conductivity; when applied in thermoelectric devices, they can effectively hinder heat transfer from the hot end to the cold end, which is conducive to establishing a larger temperature difference between the two ends of the device. Zheng *et al.* alternately embedded p-type and n-type CNT aerogels into PDMS matrices and used highly conductive silver paste to assemble flexible thermoelectric

devices[56]. Owing to advantages such as high elasticity, aerogel-based thermoelectric devices can be applied in human thermal management and sensing. Zhang *et al.* assembled graphene/PDMS aerogels prepared by a molten-salt method into functional insoles with high compressive strength and resilience; when worn, they can sense foot temperature and output 70 mV of electrical energy at 0 °C[47]. Thermoelectric arrays based on graphene/PDMS aerogels can also be used to cool computer CPUs: by absorbing heat, they reduce the operating temperature of the CPU by 8 K and convert the absorbed heat into 21 mV of electrical energy.

Structural performance comparison of f-TEGs

Based on the multi-dimensional evaluation system integrated from the literature[100,102,119], the structural performance comparison further supplements the synthesis of wearable-specific indicators. 1D fiber/yarn structures are reported to excel in weaving compatibility, with bending cycle count > 1000 cycles (R = 5 mm) and a tensile strain tolerance not less than 50%[101,102,124], making them suitable for garment integration; 2D film/ribbon structures exhibit conformal skin contact, with a reported bending stability of 500-1000 cycles and a modulus not more than 0.8 GPa[99,100], adapting to wrist/skin patches; 3D bulk/porous structures achieve high power density but relatively lower bending tolerance (300-500 cycles)[119], and are often encapsulated with biocompatible polymers (modulus not more than 1.2 GPa) for wearable use[120]. These indicators are collated from published studies on f-TEGs with different structures, clearly reflecting the relative advantages and limitations of each structure in wearable scenarios.

1D fiber/yarn f-TEGs excel in wearable integration due to their weaving compatibility, with fiber diameter and alignment affecting charge transport[3]. 2D film/ribbon structures benefit from conformal skin contact for enhanced heat transfer, and film thickness balances flexibility and thermal resistance[125-127]. 3D bulk/porous f-TEGs achieve high power density via porous structures that reduce thermal conductivity and micro-bulk units that retain high *ZT* values[56,90].

The key factors influencing the structure-performance correlations are as follows. 2D films and 3D porous structures achieve intimate contact with human skin, minimizing parasitic thermal resistance and enhancing effective temperature gradient utilization. 1D fibers and 2D films exhibit low modulus, enabling excellent bending stability that meets the requirements of repeated deformation during daily wear. 1D fibers are compatible with textile weaving processes, while 2D films can be produced via roll-to-roll coating, both supporting large-scale manufacturing and reducing production costs[100,106]. 3D bulk units and aligned 1D fibers minimize carrier scattering at the interfaces, ensuring high electrical conductivity and power density[92,122]. These comparisons provide a clear reference for structural selection of f-TEGs based on specific wearable application requirements[128,129].

Application principles

To address the lack of clear performance benchmarks in existing wearable application discussions, Table 2 establishes key benchmarks for typical application scenarios and summarizes adaptation principles to guide the design of f-TEGs. The core adaptation principles are as follows. (1) The output power of f-TEGs should match the minimum driving requirement of target devices to avoid overdesign and unnecessary material consumption[12,13]; (2) For long-term wearable scenarios (e.g., smart garments, insoles), comfort indicators (thickness, air permeability, stretchability) are prioritized to ensure user acceptance[101,102]; (3) Structural design should be optimized according to environmental characteristics (e.g., insoles require compressive resistance, masks require air permeability, wristbands require conformal contact)[47,100,122].

CONCLUSIONS

This review aims to systematically summarize the research progress of flexible thermoelectric materials and wearable thermoelectric generators, clarify the intrinsic correlations between material design, device architecture, and application scenarios, and provide theoretical and technical references for practical flexible

Table 2. Performance benchmarks and adaptation principles for typical wearable scenarios

Application scenario	Minimum driving power requirement	Wearing comfort indicators (key metrics)	Adapted f-TEG structure
Wristband sensors	1-10 μW	Thickness < 2 mm; Tensile strain > 20%	2D film + flexible substrate
Respiratory masks	0.1-1 μW	Air permeability > 50 $L \cdot m^{-2} \cdot s^{-1}$; Weight < 5 g	1D fiber/yarn textile
Smart textiles (garments)	10-100 μW	Washability > 50 cycles; Stretchability > 50%	3D porous + 1D fiber composite
Smart insoles	50-200 μW	Compressive strength > 1 MPa; Rebound rate > 80%	3D porous aerogel

1D: One-dimensional; 2D: two-dimensional; 3D: three-dimensional; f-TEG: flexible thermoelectric generators.

electronic technologies for low-grade heat harvesting. In the material aspect, it overviews the structural regulation and performance synergistic optimization strategies of inorganic nanomaterials, conducting polymers, and inorganic-organic composites, highlighting the balanced design of mechanical flexibility and thermoelectric performance. At the device level, it compares the applicable scenarios and performance trade-offs of fiber/yarn, film/ribbon, and three-dimensional bulk/porous structures, and emphasizes the core status of wearable-specific indicators such as mechanical durability and skin comfort. Meanwhile, it points out the key bottlenecks facing the current field, including the scarcity of high-performance n-type materials, insufficient long-term environmental stability, and low system integration efficiency. Future research should focus on the combination of multiscale structural design and data-driven material discovery, improve the standardized testing system under wearable scenarios, and promote the development of sustainability and clinical compatibility through interdisciplinary collaboration, facilitating the large-scale application of flexible thermoelectric technology.

DECLARATIONS

Acknowledgements

The authors acknowledge that some images in the Graphical Abstract are reproduced from the references: Copyright 2017, Royal Society of Chemistry[71]; Licensed under CC BY 4.0[72]; Copyright © 2011, Springer Nature Limited[78]; Licensed under CC BY 4.0[101]; Copyright 2022, Elsevier[106]; Copyright 2022, Elsevier[122]. Other icons and images in the Graphical Abstract are original and self-made.

Authors' contributions

Write the original draft. conceptualization, data curation, investigation, methodology: Zhu, J.; Zhou, J.
Investigation: Yang, H.; Feng, H.; Xu, M.; Chen, J.; Zhou, P.; You, M.; Shao, H.
Conceptualization, investigation, resources, supervision: Zheng, C.
Write, review & editing. conceptualization, investigation, resources, supervision: Weng, M.; Chen, H.

Availability of data and materials

Not applicable.

AI and AI-assisted tools statement

Not applicable.

Financial support and sponsorship

This work was supported by the Natural Science Foundation of Fujian Province [Grant number 2025J01999, 2023J01159], the National Natural Science Foundation of China [52201043, 62434001], College Students Innovation and Entrepreneurship Training Program of China [202510388031, S202510388042].

Conflicts of interest

Weng, M. is affiliate with Sanxiang Advanced Materials Co., Ltd. The other authors declare that there are no conflicts of interest.

Ethical approval and consent to participate

Not applicable.

Consent for publication

Not applicable.

Copyright

REFERENCES

1. Shi, X. L.; Li, N. H.; Li, M.; Chen, Z. G. Toward efficient thermoelectric materials and devices: advances, challenges, and opportunities. *Chem. Rev.* **2025**, *125*, 7525-724. DOI PubMed
2. Zhao, L. D.; Lo, S. H.; Zhang, Y.; et al. Ultralow thermal conductivity and high thermoelectric figure of merit in SnSe crystals. *Nature* **2014**, *508*, 373-7. DOI PubMed
3. Ding, T.; Chan, K. H.; Zhou, Y.; et al. Scalable thermoelectric fibers for multifunctional textile-electronics. *Nat. Commun.* **2020**, *11*, 6006. DOI PubMed PMC
4. Riffat, S.; Ma, X. Thermoelectrics: a review of present and potential applications. *Appl. Therm. Eng.* **2003**, *23*, 913-35. DOI
5. Chen, G.; Dresselhaus, M. S.; Dresselhaus, G.; Fleurial, J.; Caillat, T. Recent developments in thermoelectric materials. *Int. Mater. Rev.* **2013**, *48*, 45-66. DOI
6. Mao, D.; Yang, J.; Han, M.; et al. Homo-layer flexible Bi_2Te_3-based films with high thermoelectric performance. *Sci. Adv.* **2025**, *11*, eadz1019. DOI
7. Chen, R.; Lee, J.; Lee, W.; Li, D. Thermoelectrics of nanowires. *Chem. Rev.* **2019**, *119*, 9260-302. DOI PubMed
8. Zhang, F.; Zhao, X.; Li, R.; et al. Enhanced thermoelectric performance in high-defect SnTe alloys: a significant role of carrier scattering. *J. Mater. Chem. A.* **2022**, *10*, 23521-30. DOI
9. Deng, T.; Gao, Z.; Li, Z.; et al. Room-temperature exceptional plasticity in defective Bi_2Te_3-based bulk thermoelectric crystals. *Science* **2024**, *386*, 1112-7. DOI
10. Dolez, P. I. Energy harvesting materials and structures for smart textile applications: recent progress and path forward. *Sensors* **2021**, *21*, 6297. DOI PubMed PMC
11. Gao, J.; Shang, K.; Ding, Y.; Wen, Z. Material and configuration design strategies towards flexible and wearable power supply devices: a review. *J. Mater. Chem. A.* **2021**, *9*, 8950-65. DOI
12. Yang, S.; Li, Y.; Deng, L.; et al. Flexible thermoelectric generator and energy management electronics powered by body heat. *Microsyst. Nanoeng.* **2023**, *9*, 106. DOI PubMed PMC
13. Zhang, L.; Shi, X.; Yang, Y.; Chen, Z. Flexible thermoelectric materials and devices: from materials to applications. *Materials. Today.* **2021**, *46*, 62-108. DOI
14. Huang, S.; Qian, C.; Liu, X.; et al. A review on flexible solar cells. *Sci. China. Mater.* **2024**, *67*, 2717-36. DOI
15. Mwende Wairimu, G. Solar energy harvesting: innovations in photovoltaic materials. *Res. Invent. J. Biol. Appl. Sci.* **2024**, *3*, 64-8. https://smartie.kiu.ac.ug/public/assets/publications/d4900cbd3fe3f9868f3780d8e69aa5a4eafc1a99.pdf (accessed 2026-04-27).
16. He, Q.; Briscoe, J. Piezoelectric energy harvester technologies: synthesis, mechanisms, and multifunctional applications. *ACS. Appl. Mater. Interfaces.* **2024**, *16*, 29491-520. DOI PubMed PMC
17. Liu, H.; Zhong, J.; Lee, C.; Lee, S.; Lin, L. A comprehensive review on piezoelectric energy harvesting technology: materials, mechanisms, and applications. *Appl. Phys. Rev.* **2018**, *5*, 041306. DOI
18. Choi, G. J.; Sohn, S. H.; Kim, S. J.; Park, I. K. Polymer composite-based triboelectric nanogenerators: recent progress, design principles, and future perspectives. *Polymers* **2025**, *17*, 1962. DOI PubMed PMC
19. Iqbal, M. S.; Lu, H.; Khaladkar, S.; et al. Recent advances in triboelectric nanogenerators: mechanism, rational designing and applications. *Mater. Today. Energy.* **2024**, *46*, 101732. DOI
20. Wang, X.; Suwardi, A.; Lim, S. L.; Wei, F.; Xu, J. Transparent flexible thin-film p-n junction thermoelectric module. *npj. Flex. Electron.* **2020**, *4*, 19. DOI
21. Shakeel, M.; Rehman, K.; Ahmad, S.; Amin, M.; Iqbal, N.; Khan, A. A low-cost printed organic thermoelectric generator for low-temperature energy harvesting. *Renew. Energy.* **2021**, *167*, 853-60. DOI
22. Khoso, N. A.; Jiao, X.; GuangYu, X.; Tian, S.; Wang, J. Enhanced thermoelectric performance of graphene based nanocomposite coated self-powered wearable e-textiles for energy harvesting from human body heat. *RSC. Adv.* **2021**, *11*, 16675-87. DOI PubMed PMC
23. Hong, S.; Lee, T.; Liu, C. All-Solution-processed polythiophene/carbon nanotube nanocomposites integrated on biocompatible silk fibroin substrates for wearable thermoelectric generators. *ACS. Appl. Energy. Mater.* **2023**, *6*, 2602-10. DOI

24. Inayat, S. B.; Rader, K. R.; Hussain, M. M. Manufacturing of thermoelectric nanomaterials ($Bi_{0.4}Sb_{1.6}Te_3/Bi_{1.75}Te_{3.25}$) and integration into window glasses for thermoelectricity generation. *Energy. Tech.* **2014**, *2*, 292-9. DOI
25. Inayat, S. B.; Hussain, M. M. Power generation from thermoelectric system-embedded plexiglas for green building technology. *Appl. Nanosci.* **2012**, *3*, 335-42. DOI
26. Lee, J.; Choo, S.; Ju, H.; et al. Doping-induced viscoelasticity in PbTe thermoelectric inks for 3D printing of power-generating tubes. *Adv. Energy. Mater.* **2021**, *11*, 2100190. DOI
27. He, M.; Lin, Y.; Chiu, C.; et al. A flexible photo-thermoelectric nanogenerator based on MoS_2/PU photothermal layer for infrared light harvesting. *Nano. Energy.* **2018**, *49*, 588-95. DOI
28. Zhao, J.; Zhao, X.; Guo, R.; et al. Preparation and characterization of screen-printed Cu_2S/PEDOT:PSS hybrid films for flexible thermoelectric power generator. *Nanomaterials.* **2022**, *12*, 2430. DOI
29. Jiang, C.; Wei, P.; Ding, Y.; et al. Ultrahigh performance polyvinylpyrrolidone/Ag_2Se composite thermoelectric film for flexible energy harvesting. *Nano. Energy.* **2021**, *80*, 105488. DOI
30. Zheng, Y.; Zhang, Q.; Jin, W.; et al. Carbon nanotube yarn based thermoelectric textiles for harvesting thermal energy and powering electronics. *J. Mater. Chem. A.* **2020**, *8*, 2984-94. DOI PMC
31. Shi, X. L.; Zou, J.; Chen, Z. G. Advanced thermoelectric design: from materials and structures to devices. *Chem. Rev.* **2020**, *120*, 7399-515. DOI PubMed
32. Bahk, J.; Fang, H.; Yazawa, K.; Shakouri, A. Flexible thermoelectric materials and device optimization for wearable energy harvesting. *J. Mater. Chem. C.* **2015**, *3*, 10362-74. DOI
33. Jariwala, D.; Sangwan, V. K.; Lauhon, L. J.; Marks, T. J.; Hersam, M. C. Carbon nanomaterials for electronics, optoelectronics, photovoltaics, and sensing. *Chem. Soc. Rev.* **2013**, *42*, 2824-60. DOI PubMed
34. Yao, J.; Wang, H.; Chen, M.; Yang, M. Recent advances in graphene-based nanomaterials: properties, toxicity and applications in chemistry, biology and medicine. *Mikrochim. Acta.* **2019**, *186*, 395. DOI PubMed
35. Wang, X.; Chang, K.; Zhang, Z.; et al. Performance enhancement and mechanism exploration of all-carbon-nanotube memory with hydroxylation and dehydration through supercritical carbon dioxide. *Carbon* **2021**, *173*, 97-104. DOI
36. Huang, X.; Yu, H.; Tan, H.; et al. Carbon nanotube-encapsulated noble metal nanoparticle hybrid as a cathode material for Li-oxygen batteries. *Adv. Funct. Mater.* **2014**, *24*, 6516-23. DOI
37. Lee, M. H.; Kang, Y. H.; Kim, J.; Lee, Y. K.; Cho, S. Y. Freely shapable and 3D porous carbon nanotube foam using rapid solvent evaporation method for flexible thermoelectric power generators. *Adv. Energy. Mater.* **2019**, *9*, 1900914. DOI
38. Shi, W.; Guo, R.; Tian, G.; et al. A broadband self-powered and stable photothermoelectric detector based on Ag_2Se/MWCNTs composite fabricated via screen printing. *Microstructures* **2025**, *5*, 2025081. DOI
39. Sun, X.; Wang, Y.; Li, K.; et al. Anisotropic electrical conductivity and isotropic seebeck coefficient feature induced high thermoelectric power factor > 1800 μW m^{-1} K^{-2} in MWCNT films. *Adv. Funct. Mater.* **2022**, *32*, 2203080. DOI
40. Geim, A. K.; Novoselov, K. S. The rise of graphene. *Nat. Mater.* **2007**, *6*, 183-91. DOI PubMed PMC
41. Novoselov, K. S.; Geim, A. K.; Morozov, S. V.; et al. Electric field effect in atomically thin carbon films. *Science* **2004**, *306*, 666-9. DOI PubMed PMC
42. Kumar, V.; Kumar, A.; Lee, D. J.; Park, S. S. Estimation of number of graphene layers using different methods: a focused review. *Materials* **2021**, *14*, 4590. DOI PubMed PMC
43. Kotakoski, J.; Meyer, J. C. Mechanical properties of polycrystalline graphene based on a realistic atomistic model. *Phys. Rev. B.* **2012**, *85*, 195447. DOI
44. Cheng, C.; Li, S.; Thomas, A.; Kotov, N. A.; Haag, R. Functional graphene nanomaterials based architectures: biointeractions, fabrications, and emerging biological applications. *Chem. Rev.* **2017**, *117*, 1826-914. DOI PubMed
45. Mao, H. Y.; Laurent, S.; Chen, W.; et al. Graphene: promises, facts, opportunities, and challenges in nanomedicine. *Chem. Rev.* **2013**, *113*, 3407-24. DOI PubMed
46. Li, M.; Yin, B.; Gao, C.; et al. Graphene: preparation, tailoring, and modification. *Exploration.* **2023**, *3*, 20210233. DOI PubMed PMC
47. Zhang, D.; Mao, Y.; Bai, P.; et al. Multifunctional superelastic graphene-based thermoelectric sponges for wearable and thermal management devices. *Nano. Lett.* **2022**, *22*, 3417-24. DOI PubMed
48. Feng, S.; Yao, T.; Lu, Y.; Hao, Z.; Lin, S. Quasi-industrially produced large-area microscale graphene flakes assembled film with extremely high thermoelectric power factor. *Nano. Energy.* **2019**, *58*, 63-8. DOI
49. Guo, Y.; Mu, J.; Hou, C.; Wang, H.; Zhang, Q.; Li, Y. Flexible and thermostable thermoelectric devices based on large-area and porous all-graphene films. *Carbon* **2016**, *107*, 146-53. DOI
50. Dharmaiah, P.; Jung, S.; Kim, J.; Kim, S. K.; Baek, S. Why is it challenging to improve the thermoelectric properties of *n*-type Bi_2Te_3 alloys? *Appl. Phys. Rev.* **2024**, *11*, 031312. DOI

51. Zeng, M.; Xie, H.; Saeidi-javash, M.; et al. Scalable nanomanufacturing of chalcogenide inks: a case study on thermoelectric V-VI nanoplates. *J. Mater. Chem. A.* **2021**, *9*, 22555-62. DOI
52. Dun, C.; Kuang, W.; Kempf, N.; Saeidi-Javash, M.; Singh, D. J.; Zhang, Y. 3D printing of solution-processable 2D nanoplates and 1D nanorods for flexible thermoelectrics with ultrahigh power factor at low-medium temperatures. *Adv. Sci.* **2019**, *6*, 1901788. DOI
53. Dun, C.; Hewitt, C. A.; Li, Q.; et al. Self-assembled heterostructures: selective growth of metallic nanoparticles on V_2 -VI_3 nanoplates. *Adv. Mater.* **2017**, *29*, 1702968. DOI
54. Shi, W.; Zhou, L.; Song, S.; Yang, J.; Zhang, H. Hydrothermal synthesis and thermoelectric transport properties of impurity-free antimony telluride hexagonal nanoplates. *Adv. Mater.* **2008**, *20*, 1892-7. DOI
55. Zhou, P.; Yang, W.; Qiu, Y.; et al. Progress of MXenes-based Respons. Mater. for soft sensors and actuators. *Respons. Mater.* **2026**, *4*, e70036. DOI
56. Zheng, Z.; Li, Y.; Niu, J.; et al. Significantly (00*l*)-textured Ag_2Se thin films with excellent thermoelectric performance for flexible power applications. *J. Mater. Chem. A.* **2022**, *10*, 21603-10. DOI
57. Hu, J.; Zhu, J.; Guo, F.; et al. Electronic orbital alignment and hierarchical phonon scattering enabling high thermoelectric performance p-type Mg_3Sb_2 zintl compounds. *Research* **2022**, *2022*, 9842949. DOI
58. Park, D.; Ju, H.; Kim, J. Enhanced thermoelectric power factor and low thermal conductivity in one-dimensional Te/Ag_2Te composites. *Ceram. Int.* **2017**, *43*, 11156-62. DOI
59. Bharadwaj, S.; Ramasubramaniam, A.; Ram-Mohan, L. R. Lateral transition-metal dichalcogenide heterostructures for high efficiency thermoelectric devices. *Nanoscale* **2022**, *14*, 11750-9. DOI PubMed
60. Oh, J. Y.; Lee, J. H.; Han, S. W.; et al. Chemically exfoliated transition metal dichalcogenide nanosheet-based wearable thermoelectric generators. *Energy. Environ. Sci.* **2016**, *9*, 1696-705. DOI PMC
61. Patil, B.; Bernini, C.; Marré, D.; Pellegrino, L.; Pallecchi, I. Ink-jet printing and drop-casting deposition of 2H-phase $SnSe_2$ and WSe_2 nanoflake assemblies for thermoelectric applications. *Nanotechnology* **2021**, *33*, 035302. DOI
62. Guo, Y.; Dun, C.; Xu, J.; et al. Wearable thermoelectric devices based on au-decorated two-dimensional MoS_2. *ACS. Appl. Mater. Interfaces.* **2018**, *10*, 33316-21. DOI PubMed
63. Chen, K.; Luan, Q.; Liu, T.; Albinsson, B.; Hou, L. Semiconductor nanocrystals-based triplet-triplet annihilation photon-upconversion: mechanism, materials and applications. *Respons. Mater.* **2024**, *3*, e20240030. DOI
64. Li, J.; Shi, Q.; Röhr, J. A.; et al. Flexible 3D porous MoS_2/CNTs Architectures with *ZT* of 0.17 at room temperature for wearable thermoelectric applications. *Adv. Funct. Mater.* **2020**, *30*, 2002508. DOI
65. Shirakawa, H. The discovery of polyacetylene film: the dawning of an era of conducting polymers (Nobel Lecture). *Angew. Chem. Int. Ed.* **2001**, *40*, 2574-80. DOI
66. Heeger, A. J. Semiconducting and metallic polymers: the fourth generation of polymeric materials. *J. Phys. Chem. B.* **2001**, *105*, 8475-91. DOI
67. Li, J.; Tang, X.; Li, H.; Yan, Y.; Zhang, Q. Synthesis and thermoelectric properties of hydrochloric acid-doped polyaniline. *Synth. Met.* **2010**, *160*, 1153-8. DOI
68. Yao, Q.; Wang, Q.; Wang, L.; et al. The synergic regulation of conductivity and Seebeck coefficient in pure polyaniline by chemically changing the ordered degree of molecular chains. *J. Mater. Chem. A.* **2014**, *2*, 2634-40. DOI
69. Yao, Q.; Chen, L.; Xu, X.; Wang, C. The High thermoelectric properties of conducting polyaniline with special submicron-fibre structure. *Chem. Lett.* **2005**, *34*, 522-3. DOI
70. Cho, C.; Wallace, K. L.; Tzeng, P.; Hsu, J. H.; Yu, C.; Grunlan, J. C. Outstanding low temperature thermoelectric power factor from completely organic thin films enabled by multidimensional conjugated nanomaterials. *Adv. Energy. Mater.* **2016**, *6*, 1502168. DOI
71. Liang, L.; Chen, G.; Guo, C. Polypyrrole nanostructures and their thermoelectric performance. *Mater. Chem. Front.* **2017**, *1*, 380-6. DOI
72. Zhao, X.; Xu, H.; Liu, Z. T.; Li, G.; Jiang, J.; Liu, Z. W. Designable polypyrrole pattern in hydrogel achieved by photo-controllable concentration of Fe^{3+} initiator. *Smart. Mol.* **2024**, *2*, e20240015. DOI
73. Wang, J.; Cai, K.; Shen, S.; Yin, J. Preparation and thermoelectric properties of multi-walled carbon nanotubes/polypyrrole composites. *Synth. Met.* **2014**, *195*, 132-6. DOI
74. Park, H.; Kim, J. W.; Hong, S. Y.; et al. Microporous polypyrrole-coated graphene foam for high-performance multifunctional sensors and flexible supercapacitors. *Adv. Funct. Mater.* **2018**, *28*, 1707013. DOI
75. Song, H.; Cai, K.; Wang, J.; Shen, S. Influence of polymerization method on the thermoelectric properties of multi-walled carbon nanotubes/polypyrrole composites. *Synth. Met.* **2016**, *211*, 58-65. DOI
76. Groenendaal, L.; Jonas, F.; Freitag, D.; et al. Poly (3, 4-ethylenedioxythiophene) and its derivatives: past, present, and future. *Adv. Mater.* **2000**, *12*, 481-94. DOI

77. Hu, X.; Chen, G.; Wang, X.; Wang, H. Tuning thermoelectric performance by nanostructure evolution of a conducting polymer. *J. Mater. Chem. A.* **2015**, *3*, 20896-902. DOI
78. Bubnova, O.; Khan, Z. U.; Malti, A.; et al. Optimization of the thermoelectric figure of merit in the conducting polymer poly(3,4-ethylenedioxythiophene). *Nat. Mater.* **2011**, *10*, 429-33. DOI
79. Kim, J.; Jung, J.; Lee, D.; Joo, J. Enhancement of electrical conductivity of poly(3,4-ethylenedioxythiophene)/poly(4-styrenesulfonate) by a change of solvents. *Synth. Met.* **2002**, *126*, 311-6. DOI
80. Ouyang, J.; Xu, Q.; Chu, C.; Yang, Y.; Li, G.; Shinar, J. On the mechanism of conductivity enhancement in poly(3,4-ethylenedioxythiophene):poly(styrene sulfonate) film through solvent treatment. *Polymer* **2004**, *45*, 8443-50. DOI
81. Jönsson, S.; Birgerson, J.; Crispin, X.; et al. The effects of solvents on the morphology and sheet resistance in poly(3,4-ethylenedioxythiophene)-polystyrenesulfonic acid (PEDOT-PSS) films. *Synth. Met.* **2003**, *139*, 1-10. DOI
82. Kee, S.; Kim, N.; Kim, B. S.; et al. Controlling molecular ordering in aqueous conducting polymers using ionic liquids. *Adv. Mater.* **2016**, *28*, 8625-31. DOI
83. Fan, Z.; Du, D.; Yao, H.; Ouyang, J. Higher PEDOT molecular weight giving rise to higher thermoelectric property of PEDOT:PSS: a comparative study of clevios p and clevios PH1000. *ACS. Appl. Mater. Interfaces.* **2017**, *9*, 11732-8. DOI PubMed
84. Petsagkourakis, I.; Pavlopoulou, E.; Cloutet, E.; et al. Correlating the Seebeck coefficient of thermoelectric polymer thin films to their charge transport mechanism. *Organic. Electronics.* **2018**, *52*, 335-41. DOI
85. Wei, Q.; Mukaida, M.; Kirihara, K.; Naitoh, Y.; Ishida, T. Thermoelectric power enhancement of PEDOT:PSS in high-humidity conditions. *Appl. Phys. Express.* **2014**, *7*, 031601. DOI
86. Wang, H.; Ail, U.; Gabrielsson, R.; Berggren, M.; Crispin, X. Ionic Seebeck effect in conducting polymers. *Adv. Energy. Mater.* **2015**, *5*, 1500044. DOI
87. Liu, P.; Li, Y.; Ni, Z.; Guo, C. Recent advances in preparation, thermoelectric properties, and applications of organic small molecule/SWCNT composites. *Microstructures* **2024**, *4*, 2024061. DOI
88. Li, D.; Wu, G.; Wang, X.; Wu, J. R.; Yang, Y. W. [2]Biphenyl-extended pillar[6]arene functionalized silver nanoparticles for catalysis and label-free detection. *Smart. Mol.* **2023**, *1*, e20230016. DOI
89. Zhang, Y.; Hu, Y.; Xie, B.; Yang, G.; Yin, Z.; Wu, H. Hoffmeister effect optimized hydrogel electrodes with enhanced electrical and mechanical properties for nerve conduction studies. *Research* **2024**, *7*, 0453. DOI PubMed PMC
90. Cohn, J. L.; Nolas, G. S.; Fessatidis, V.; Metcalf, T. H.; Slack, G. A. Glasslike heat conduction in high-mobility crystalline semiconductors. *Phys. Rev. Lett.* **1999**, *82*, 779-82. DOI
91. Weng, M.; Qiu, Y.; Zhou, J.; et al. Multi-functional $Nb_4C_3T_x$ (MXene)-bacterial cellulose composites for multimodal self-powered sensors toward a material/temperature recognition system. *Chem. Eng. J.* **2025**, *522*, 167607. DOI
92. Zhang, J.; Zhang, T.; Zhang, H.; et al. Single-crystal SnSe thermoelectric fibers via laser-induced directional crystallization: from 1D fibers to multidimensional fabrics. *Adv. Mater.* **2020**, *32*, e2002702. DOI
93. Chen, C.; Zhao, B.; Wang, R.; et al. Janus helical ribbon structure of ordered nanowire films for flexible solar thermoelectric devices. *Adv. Mater.* **2022**, *34*, e2206364. DOI PubMed
94. Zhao, Z.; Fu, H.; Tang, R.; Zhang, B.; Chen, Y.; Jiang, J. Failure mechanisms in flexible electronics. *Int. J. Smart. Nano. Mater.* **2023**, *14*, 510-65. DOI
95. Li, J.; Meng, X.; Shen, Y.; et al. Design strategy of porous elastomer substrate and encapsulation for inorganic stretchable electronics. *Int. J. Smart. Nano. Mater.* **2024**, *15*, 330-47. DOI
96. Gao, Y.; Xu, J.; Qu, S.; Li, Y.; Sukhorukov, G. B.; Shang, L. Mussel-inspired self-assembly of silver nanoclusters into multifunctional silver aerogels for enhanced catalytic and bactericidal applications. *Exploration.* **2025**, *5*, 20240034. DOI
97. Zhou, S. W.; Yu, C.; Chen, M.; Shi, C. Y.; Gu, R.; Qu, D. H. Self-healing and shape-shifting polymers controlled by dynamic bonds. *Smart. Mol.* **2023**, *1*, e20220009. DOI
98. Yang, B.; Zhu, X.; Peng, C.; et al. Synchronized measurement of electromechanical responses of fabric strain sensors under large deformation. *Smart. Wearable. Technol.* **2025**, *1*, A7. DOI
99. Wang, X.; Liu, T.; Sun, F.; et al. Highly tough, crack-resistant and self-healable piezo-ionic skin enabled by dynamic hard domains with mechanosensitive ionic channel. *Smart. Mol.* **2024**, *2*, e20240008. DOI
100. Na, Y.; Kim, S.; Mallem, S. P. R.; Yi, S.; Kim, K. T.; Park, K. Energy harvesting from human body heat using highly flexible thermoelectric generator based on Bi_2Te_3 particles and polymer composite. *J. Alloys. Compd.* **2022**, *924*, 166575. DOI
101. Sun, T.; Zhou, B.; Zheng, Q.; Wang, L.; Jiang, W.; Snyder, G. J. Stretchable fabric generates electric power from woven thermoelectric fibers. *Nat. Commun.* **2020**, *11*, 572. DOI PubMed PMC
102. Lee, J. A.; Aliev, A. E.; Bykova, J. S.; et al. Woven-yarn thermoelectric textiles. *Adv. Mater.* **2016**, *28*, 5038-44. DOI
103. Dai, Z.; Lei, M.; Ding, S.; et al. Durable superhydrophobic surface in wearable sensors: from nature to application. *Exploration* **2024**, *4*, 20230046. DOI PubMed PMC

104. Komatsu, N.; Ichinose, Y.; Dewey, O. S.; et al. Macroscopic weavable fibers of carbon nanotubes with giant thermoelectric power factor. *Nat. Commun.* **2021**, *12*, 4931. DOI PubMed PMC
105. Li, C.; Wang, T.; Zhou, S.; et al. Deep learning model coupling wearable bioelectric and mechanical sensors for refined muscle strength assessment. *Research* **2024**, *7*, 0366. DOI PubMed PMC
106. He, X.; Gu, J.; Hao, Y.; et al. Continuous manufacture of stretchable and integratable thermoelectric nanofiber yarn for human body energy harvesting and self-powered motion detection. *Chem. Eng. J.* **2022**, *450*, 137937. DOI
107. Fu, S.; Cheng, X.; Liu, J.; et al. An ultra-stretchable fiber sensor with high linearity and durability via thermal drawing. *Int. J. Smart. Nano. Mater.* **2024**, *16*, 144-59. DOI
108. Zhang, T.; Li, K.; Zhang, J.; et al. High-performance, flexible, and ultralong crystalline thermoelectric fibers. *Nano. Energy.* **2017**, *41*, 35-42. DOI
109. Xu, Z.; Zhang, F.; Xie, E.; et al. A flexible, large-scale sensing array with low-power in-sensor intelligence. *Research* **2024**, *7*, 0497. DOI PubMed PMC
110. Ren, H.; Li, W.; Ding, Y.; et al. Flexible tactile sensors for enhancing robotic perception. *Smart. Wearable. Technol.* **2025**, *1*, A2. DOI
111. Zhang, P.; Wang, G.; Yu, H. Ultraviolet-visible-near-infrared light-responsive soft materials: fabrication, photomechanical deformation and applications. *Respons. Mater.* **2024**, *2*, e20240016. DOI
112. Wei, L.; Liu, X.; Li, Y.; et al. Multifunctional PHC bandage for accelerated wound healing in movable parts. *Exploration.* **2025**, *5*, 20230176. DOI PubMed PMC
113. Nan, K.; Kang, S. D.; Li, K.; et al. Compliant and stretchable thermoelectric coils for energy harvesting in miniature flexible devices. *Sci. Adv.* **2018**, *4*, eaau5849. DOI PubMed PMC
114. Chen, C.; Wang, R.; Li, X. L.; et al. Structural design of nanowire wearable stretchable thermoelectric generator. *Nano. Lett.* **2022**, *22*, 4131-6. DOI PubMed
115. Lu, Y.; Qu, X.; Zhao, W.; et al. Highly stretchable, elastic, and sensitive MXene-based hydrogel for flexible strain and pressure sensors. *Research.* **2020**, *2020*, 2038560. DOI PubMed PMC
116. Chiba, S.; Waki, M. The potential of wearable systems using dielectric elastomers (DE). *Smart. Wearable. Technol.* **2025**, *1*, A3. DOI
117. Zhu, P.; Shi, C.; Wang, Y.; et al. Recyclable, healable, and stretchable high-power thermoelectric generator. *Adv. Energy. Mater.* **2021**, *11*, 2100920. DOI
118. Kim, S.; Hyeon, D. Y.; Ham, S. S.; et al. Synergetic enhancement of the energy harvesting performance in flexible hybrid generator driven by human body using thermoelectric and piezoelectric combine effects. *Appl. Surf. Sci.* **2021**, *558*, 149784. DOI
119. Kim, S. J.; We, J. H.; Cho, B. J. A wearable thermoelectric generator fabricated on a glass fabric. *Energy. Environ. Sci.* **2014**, *7*, 1959. DOI PMC
120. Sargolzaeiaval, Y.; Padmanabhan Ramesh, V.; Neumann, T. V.; et al. Flexible thermoelectric generators for body heat harvesting - enhanced device performance using high thermal conductivity elastomer encapsulation on liquid metal interconnects. *Appl. Energy.* **2020**, *262*, 114370. DOI
121. Yuan, J.; Zhu, R. A fully self-powered wearable monitoring system with systematically optimized flexible thermoelectric generator. *Appl. Energy.* **2020**, *271*, 115250. DOI
122. Xu, Q.; Deng, B.; Zhang, L.; et al. High-performance, flexible thermoelectric generator based on bulk materials. *Cell. Rep. Phys. Sci.* **2022**, *3*, 100780. DOI
123. Liang, J.; Wang, T.; Qiu, P.; et al. Flexible thermoelectrics: from silver chalcogenides to full-inorganic devices. *Energy. Environ. Sci.* **2019**, *12*, 2983-90. DOI PMC
124. Jeon, J.; Bukharina, D.; Kim, M.; et al. Tunable and responsive photonic bio-inspired materials and their applications. *Respons. Mater.* **2024**, *2*, e20230032. DOI
125. Kumar, S.; Battabyal, M.; Satapathy, D. K. Flexible Ag_2Se film with enhanced thermoelectric performance. *ACS. Appl. Mater. Interfaces.* **2024**, *16*, 66170-80. DOI PubMed
126. Chen, W.; Shi, X. L.; Li, M.; et al. Nanobinders advance screen-printed flexible thermoelectrics. *Science* **2024**, *386*, 1265-71. DOI PubMed
127. Yi, N.; Zhang, C.; Wang, Z.; et al. Multi-functional $Ti_3C_2T_x$-silver@silk nanofiber composites with multi-dimensional heterogeneous structure for versatile wearable electronics. *Adv. Funct. Mater.* **2024**, *35*, 2412307. DOI
128. Zhang, L.; Qin, P.; Ying, H.; et al. A 3.55-μm Ultrathin, skin-like mechanoresponsive, compliant, and seamless ionic conductive electrode for epidermal electrophysiological signal acquisition and human-machine interaction. *Exploration* **2025**, *5*, 20240232. DOI
129. Lee, J. H.; Hong, K. I.; Choi, W. H.; Kim, Y.; Jang, W. D. Triazole-bearing oligo(ethylene glycol)-strapped zinc porphyrins as dual mode ion-binding receptors. *Smart. Mol.* **2023**, *1*, e20220004. DOI